OCA-B promotes autoimmune demyelination through control of stem-like CD4+ T cells

Erik P. Hughes[1,3], Amber R. Syage[1,3], Elnaz Mirzaei Mehrabad[2,3,4], Thomas E. Lane[5], Benjamin T. Spike[2,3], Dean Tantin[1,3]

[1]Department of Pathology, University of Utah School of Medicine, Salt Lake City, UT 84112 U.S.A.
[2]Department of Oncological Sciences, University of Utah School of Medicine, Salt Lake City, UT 84112 U.S.A.
[3]Huntsman Cancer Institute, University of Utah School of Medicine, Salt Lake City, UT 84112 U.S.A.
[4]School of Computing, University of Utah, Salt Lake City, UT, 84112 U.S.A
[5]Department of Neurobiology and Behavior, School of Biological Sciences, University of California, Irvine, CA 92697, U.S.A.
e-mail dean.tantin@path.utah.edu

Short title: OCA-B promotes CD4+ T cell mediated demyelinating disease

Keywords OCA-B/Bob1/Pou2af1; autoimmunity; multiple sclerosis; EAE; stem-like CD4+ T cells; relapsing-remitting

Words in abstract: 166
Words main text: 4,648
Total main display items: 6

Summary

Stem-like T cell populations can selectively contribute to autoimmunity, but the activities that promote and sustain these populations are incompletely understood. Here, we show that T cell-intrinsic loss of the transcription cofactor OCA-B protects mice from experimental autoimmune encephalomyelitis (EAE) while preserving responses to CNS infection. In adoptive transfer EAE models driven by multiple antigen encounters, OCA-B deletion nearly eliminates CNS infiltration, proinflammatory cytokine production and clinical disease. OCA-B-expressing $CD4^+$ T cells within the CNS of mice with EAE comprise a minority of the population but display a memory phenotype and preferentially confer disease. In a relapsing-remitting EAE model, OCA-B T cell deficiency specifically protects mice from relapse. During remission, OCA-B promotes the expression of *Tcf7*, *Slamf6*, and *Sell* in proliferating T cell populations. At relapse, OCA-B loss results in both the accumulation of an immunomodulatory $CD4^+$ T cell population expressing *Ccr9* and *Bach2*, and the loss of pro-inflammatory gene expression from Th17 cells. These results identify OCA-B as a driver of pathogenic stem-like T cells.

Introduction

2.5 million individuals worldwide suffer from multiple sclerosis (MS), with almost 1 million cases in the United States[1]. Despite recent advances, the development of new therapies that block MS while sparing immunosurveillance mechanisms needed to prevent infection and viral recrudescence remains a critical goal. Genome-wide association studies (GWAS) identify the *HLA* loci as the most important determinant of MS pathogenesis, emphasizing the impact of T cells in MS[2,3]. The association with the major histocompatibility complex (MHC) class II locus in particular indicates that myelin-specific $CD4^+$ T cells are key regulators of disease.

The predominant preclinical model of MS is experimental autoimmune encephalomyelitis (EAE), in which laboratory animals are immunized with myelin-specific proteins or peptides to activate antigen specific $CD4^+$ T cells that infiltrate the central nervous system (CNS) and mediate disease. EAE within the C57BL/6 mouse background establishes chronic disease. In these models, Th1 and Th17 effector $CD4^+$ T cell subsets are pathogenetic mediators[4,5]. After accessing the CNS, these cells promote neuroinflammation through the secretion of interferon-gamma (IFNγ), interleukin-17 (IL-17), granulocyte macrophage stimulating-factor (GM-CSF) and other inflammatory mediators and chemoattractants that recruit the cell types responsible for driving demyelination[6–8].

Myelin-reactive T cells from the blood of MS patients show stem/memory-like properties, with reduced need for co-stimulation, suggesting signs of previous activation[9–12]. Consistent with these findings, autoreactive and bystander memory-phenotype $CD4^+$ T cells preferentially transfer demyelinating disease in mouse models[13–15]. While these studies have identified vital $CD4^+$ T cell populations in EAE, further research on the mechanisms creating and sustaining these populations is required to develop more precise therapies.

Oct1, a POU domain transcription factor encoded by *Pou2f1*, has been linked to autoimmune states. GWAS studies have identified Oct1 binding site polymorphisms that associate with a predisposition for autoimmune diseases, including MS[16–19]. In $CD4^+$ T cells, Oct1 promotes the development of both $CD4^+$ memory[20] and EAE pathogenesis and demyelination[21]. In contrast, Oct1 loss preserves immune responses to the neurotrophic viral infection[21]. These observations highlight a promising therapeutic window in which targeting this pathway may limit autoimmune CNS demyelination without the broad immune suppression elicited by many current therapeutics. However, Oct1 is widely expressed and regulates both embryonic development and somatic stem cell function[22–24], making it a poor therapeutic target.

The lymphoid-restricted transcription cofactor OCA-B regulates transcription by docking with Oct1, and in B cells an additional related factor, Oct2[25]. In contrast to Oct1, OCA-B whole-

79 body knockouts are viable and fertile[26]. Polymorphisms in the *Ocab* (*Pou2af1*) locus are
80 associated with autoimmune diseases, including MS[27,28]. Although its expression is 50-100 fold
81 lower in T cells compared to B cells[29], targeting either OCA-B by genetic deletion in T cells or its
82 downstream pathways with a membrane-permeable peptide mimic suppresses type-1 diabetes[31].
83 OCA-B interacts with target genes such as *Il2, Ifng, Il21, Csf2 (Gmcsf), Tnfrsf4 (Ox40), Icos* and
84 *Ctla4*, but is dispensable for their expression following primary activation of T cells. Instead, OCA-
85 B regulates these targets under a narrow range of conditions, for example following secondary
86 stimulation in culture[20]. Many of these targets are directly implicated in MS pathogenesis[6–8,31–37].
87 OCA-B controls expression of *Tbx21* (*Tbet*), which encodes a key regulator of Th1 effector
88 responses, but also promotes Th17 differentiation and interacts with RORγt, a master regulator
89 of Th17 cells[20,38,39]. In the context of MS, the only published OCA-B work used whole body
90 knockouts and showed measurable but incomplete protection in chronic C57BL/6 EAE models[39].
91 Cumulatively, these findings indicate that OCA-B plays poorly defined but possibly significant
92 roles in MS pathogenesis.
93 Here, we show that OCA-B within the T cell compartment drives EAE by promoting
94 pathogenic maturation of stem-like $CD4^+$ T cells. In C57BL/6 mice, T cell OCA-B loss significantly
95 protects mice from chronic EAE, while preserving responses to the neurotrophic coronavirus
96 JHMV. Using Th1 and Th17 passive transfer assays in which reactive T cells encounter antigen
97 in donor mice, in polarizing culture, and again in naïve recipients, we show that OCA-B is essential
98 for the infiltration of pathogenic cells into the CNS and the manifestation of clinical disease. Using
99 an OCA-B reporter mouse, we find that OCA-B expressing $CD4^+$ T cells taken from MOG peptide
100 primed mice display pathogenic stem-like gene expression and preferentially transfer
101 demyelinating disease, highlighting OCA-B as a marker and promoter of encephalitogenic
102 autoimmune $CD4^+$ T cell activity. Intriguingly, T cell conditional OCA-B knockout In EAE models
103 on the autoimmune-prone non-obese diabetic (NOD) background, which develops a relapsing-
104 remitting disease[40], specifically protects against relapse. Single-cell transcriptomic analysis of
105 $CD3\varepsilon^+$ CNS-infiltrating T cells at remission and relapse indicates that OCA-B promotes disease
106 relapse through control of stem-like T cell populations, driving them to pathogenic Th17
107 differentiation. Cumulatively, these findings mark OCA-B as a critical mediator of the pathogenic
108 maturation of autoreactive T cells, and a promising potential therapeutic target.

Results

OCA-B promotes chronic EAE in C57BL/6 mice

To understand the impact of OCA-B in T cell mediated autoimmunity, we utilized an *Ocab* (*Pou2af1*) conditional knockout allele crossed to the CD4-Cre driver which efficiently deletes OCA-B in T cells[30]. We induced EAE in C57BL/6 female *Ocab*$^{fl/fl}$;CD4-Cre mice and littermate *Ocab*$^{fl/fl}$ controls through subcutaneous (s.c.) injection of myelin oligodendrocyte glycoprotein $(MOG)_{35-55}$ peptide in Complete Freund's Adjuvant (CFA) followed by intraperitoneal (i.p.) injections of *Bordetella pertussis* toxin. *Ocab*$^{fl/fl}$;CD4-Cre mice showed reduced chronic EAE clinical scores and weight loss compared to *Ocab*$^{fl/fl}$ littermate controls (Fig. 1a, b). Spinal cords were taken at peak disease (day 15) for immunofluorescence and histological analysis. Myelin basic protein (MBP) immunofluorescence showed a significant decrease in demyelinated white matter in spinal sections from Ocab$^{fl/fl}$;CD4-Cre mice compared to littermate Ocab$^{fl/fl}$ controls while DAPI showed decreased immune cell infiltration (Fig. 1c, d). Similarly, Ocab$^{fl/fl}$;CD4-Cre mice showed a small but significant decrease in demyelination as measured by luxol fast blue (LFB) in combination with hematoxylin and eosin (H&E) staining (Extended Data Fig. 1a, b). Peak disease flow cytometric profiling showed decreased CD4$^+$ T cell infiltration into the CNS of *Ocab*$^{fl/fl}$;CD4-Cre mice, however no differences in other infiltrating cell populations or in the relative proportions of the proinflammatory cytokines IFNy, IL-17, GM-CSF, or CD44 were observed (Fig. 1e, f, and Extended Data Fig. 1c-h). As no differences in the frequency of cytokine expression were observed across total T cell populations, we studied MOG-specific CD4$^+$ T cells using the MHC class II I-A^b MOG_{38-49} tetramers. At peak disease, *Ocab*$^{fl/fl}$;CD4-Cre mice showed a trending reduction in CD44$^+$ MOG tetramer-specific cell frequency (p=0.0637) and a significant reduction in numbers (p=0.003) compared to controls (Fig. 1g, h). These results indicate that the protection conferred by OCA-B loss in T cells is marked by modest decreases in MOG-specific CD4$^+$ T cells within the CNS, resulting in fewer pathogenic T cells driving demyelination.

OCA-B is essential for EAE mediated by adoptive transfer of Th1- and Th17-polarized T cells

MS is driven by autoreactive CD4$^+$ Th1 and Th17 cells within the CNS that recruit CD8$^+$ T cells, macrophages, microglia and neutrophils, which together mediate white-matter damage[41]. To investigate the impact of OCA-B on autoimmune Th1 and Th17 populations, we used adoptive transfer EAE models with female *Ocab*$^{fl/fl}$;CD4-Cre and *Ocab*$^{fl/fl}$ littermate controls. Mice were primed with MOG_{35-55} in CFA for 10-14 days. Following MOG priming, no differences between

142 genotypes in CD4$^+$ T cell viability, count, or effector cytokine (IFNγ and IL-17) expression were
143 observed (Extended Data Fig. 2a-e). Interestingly, CD4$^+$ T cells from Ocab$^{fl/fl}$;CD4-Cre mice
144 showed a modest increase in the percentage of cells expressing Ki67 compared to Ocab$^{fl/fl}$
145 littermate controls (Extended Data Fig. 2f). To determine differences in adoptive transfer viability
146 and proliferation, CD4$^+$ T cells from MOG$_{35-55}$ primed Ocab$^{fl/fl}$ control and Ocab$^{fl/fl}$;CD4-Cre
147 experimental donors were labeled with fluorescent quantum dots (Ocab$^{fl/fl}$-QTracker 655 and
148 Ocab$^{fl/fl}$;CD4-Cre-QTracker 525), combined 1:1 and transferred into naïve recipients. Three days
149 following mixed transfer, cell were recovered from the peritoneal cavities. The frequency of
150 Ocab$^{fl/fl}$;CD4-Cre donor CD4$^+$ T cells in the peritoneal cavity was decreased and showed
151 diminished viability compared to control donor CD4$^+$ T cells (Extended Data Fig. 2g-j). Similar to
152 cells collected before transfer, CD4$^+$ T cells from Ocab$^{fl/fl}$;CD4-Cre donors showed a significant
153 increase in Ki67 expression (Extended Data Fig. 2k, l). The combination of decreased numbers
154 and increased proliferation in transferred OCA-B knockout T cells may reflect preferential homing
155 of these cells to tissues such as the gut.
156 To investigate if OCA-B expression impacts Th1 or Th17 mediated adoptive transfer EAE,
157 CD4$^+$ T cells were purified from the lymph nodes of primed experimental or control donors and
158 polarized in vitro into Th1 and Th17 cells as previously described[42,43]. 3×10^6 Th1- or Th17-
159 polarized CD4$^+$ cells were transferred into naïve age-matched wild-type male C57BL/6 recipients
160 by i.p. injection. EAE onset in mice receiving either Th1- or Th17-polarized control cells was rapid
161 and severe (Fig. 2a, b). In contrast to the mild protection observed with OCA-B deficiency in
162 standard C57BL/6 EAE, mice adoptively transferred with T cells lacking OCA-B were almost
163 completely protected from clinical disease regardless of their polarization state. Interestingly, the
164 ability to initially polarize CD4$^+$ T cells into Th1 and Th17 effectors in vitro was minimally affected
165 by OCA-B loss (Extended Data Fig. 2m-o), whereas the same cells taken from the CNS of Th17-
166 engrafted recipient mice at day 15 not only showed decreased CNS infiltration but also poor IL-
167 17 expression (Fig. 2c-f). This effect appeared to be specific to IL-17, as no significant difference
168 in IFNγ expression was observed (Extended Data Fig. 2p) These results indicate a central role for
169 OCA-B in promoting robust neuroinflammatory T cell responses upon antigen reencounter in
170 adoptive transfer EAE models.
171
172 **OCA-B is dispensable for neurotropic viral clearance**

173 To investigate if T cell OCA-B deletion impacts the ability to mount immune responses and control
174 viral infection in the CNS, male *Ocab*$^{fl/fl}$;CD4-Cre and *Ocab*$^{fl/fl}$ littermate controls were intracranially
175 inoculated with 1500 plaque-forming units (PFU) of the John H. Muller strain of murine hepatitis
176 virus (JHMV), a β-coronavirus adapted to infect glial cells (astrocytes, microglia and
177 oligodendrocytes) in the mouse brain and spinal cord. Inoculation with JHMV results in acute
178 encephalomyelitis and chronic demyelination similar to autoantigen-driven EAE but without
179 persistent autoantigen. Disease severity was determined by evaluating JHMV clinical scores over
180 21 days post-infection (dpi). *Ocab*$^{fl/fl}$;CD4-Cre animals showed negligible differences in clinical
181 scores compared to *Ocab*$^{fl/fl}$ littermates (Fig. 3a), suggesting that OCA-B loss preserves baseline
182 T cell responses to acute infection. Spinal cords were taken on 12 and 21 dpi for
183 immunofluorescence and histological analysis to investigate differences in demyelination. MBP
184 immunofluorescence at 12 dpi showed similar demyelination and immune infiltration in both
185 Ocab$^{fl/fl}$ and Ocab$^{fl/fl}$;CD4-Cre spinal sections (Fig. 3b, c). Similarly, LFB histology of brain tissue
186 at 21 dpi showed no significant differences in demyelination between OCA-B deficient and control
187 infected animals (Extended Data Fig. 3a, b). Flow cytometric analysis of brain tissue showed no
188 significant differences in infiltrating CD4$^+$ T cell numbers or their ability to express IFNγ at 7, 12,
189 and 21 dpi (Fig. 3d-f, and Extended Data Fig. 3c). Similarly, no differences in either the total
190 numbers of CD8$^+$ T cells, or the percent expression or numbers of IFNγ expressing CD8$^+$ T cells
191 was observed (Extended Data Fig. 3d-f). Brain homogenates were collected on 7, 12 and 21 dpi
192 to measure viral titers and clearance. *Ocab*$^{fl/fl}$;CD4-Cre and *Ocab*$^{fl/fl}$ littermate control animals
193 showed similar titers at dpi 7 and 12, and virus was undetectable at day 21 regardless of genotype
194 (Fig. 3g). This result suggests that OCA-B is dispensable for immune responses to and clearance
195 of neurotropic viruses.
196

197 **OCA-B expressing CD4$^+$ T cells display pathogenic stem-like properties and preferentially**
198 **transfer demyelinating disease**

199 We used a recently described an OCA-B reporter (OCA-B-mCherry) mouse which selectively
200 labels OCA-B expressing B and T cells with mCherry[29] to evaluate OCA-B expression within CNS
201 infiltrating T cells. EAE was induced in female C57BL/6 homozygous OCA-B-mCherry reporter
202 mice with MOG_{35-55}, and CNS-infiltrating CD4$^+$ T cells assessed by flow cytometry at peak clinical
203 disease. mCherry-positive cells showed increased CD44 and CD62L co-expression, indicative of
204 memory-like properties in the OCA-B expressing T cell population (Fig. 4a). The association of

205 OCA-B expression with a memory-like profile was observed in the brain, spine and draining
206 cervical lymph nodes (Fig. 4b). Interestingly, the frequency of $CD44^{+}CD62L^{-}CD4^{+}$ T cells was
207 elevated within the OCA-B expressing population specifically within the cervical lymph nodes
208 (Extended Data Fig. 4a).

209 Memory-like $CD4^{+}$ T cells have been implicated as major orchestrators of autoimmune
210 demyelination in mice and humans[9–12,14,15,44]. To see if this memory-like profile of OCA-B
211 expressing $CD4^{+}$ T cells is specific to CNS infiltrating cells, we performed flow cytometry using
212 draining lymph node and splenic T cells from MOG-primed OCA-B-mCherry reporter mice. Similar
213 to OCA-B^{+} CNS infiltrating cells, OCA-B expressing $CD4^{+}$ T cells taken from the cervical lymph
214 node and spleen showed increased CD44 and CD62L co-expression (Fig. 4c, d).

215 We next evaluated OCA-B-mCherry positive and negative populations by RNA
216 sequencing of $CD4^{+}$ T cells isolated from the lymph nodes of 14-day MOG-primed mice. ~1500
217 genes were upregulated and ~350 downregulated in OCA-B expressing compared to OCA-B
218 negative cells (Supplementary Table 1). Upregulated genes in OCA-B expressing cells included
219 *Cxcr6*, *Slamf6*, *Il23r*, *Rorc*, *Ifng*, and *Il17a* while downregulated genes included *Foxp3*, *Il7r* and
220 *Ccr9* (Fig. 4e, f). Expression of *Tcf7* (which encodes TCF1) was high within both OCA-B positive
221 and negative populations (Supplementary Table 1). Gene ontology (GO) and pathway analysis of
222 upregulated genes show enrichment for terms associated with autoimmune diseases including
223 lupus, autoimmune thyroid disease, and type-1 diabetes (Fig. 4g, and Supplementary Table 2).

224 To determine if OCA-B expression can be used to prospectively identify viable pathogenic
225 $CD4^{+}$ T cell populations, we used OCA-B-mCherry reporter mice as donors in passive transfer
226 EAE. 11-week-old male and female littermates homozygous for the OCA-B-mCherry reporter
227 were primed for 14 days with $MOG_{35\text{-}55}$ in CFA as previously described[43]. $CD4^{+}$ T cells were
228 isolated from spleen and lymph nodes and sorted based on mCherry expression (Extended Data
229 Fig. 4b). 9×10^{5} mCherry negative and positive cells were cultured in Th1 polarizing conditions and
230 subsequently transferred into age-matched male C57BL/6 recipients as previously described[14].
231 Disease progression was measured by clinical score and normalized weight. Recipients of OCA-
232 B-expressing mCherry positive cells showed increased clinical disease severity and weight loss
233 compared to mCherry negative recipients (Fig. 4h, and Extended Data Fig. 4c). These findings
234 indicate that OCA-B marks $CD4^{+}$ T cells with pathogenic stem-like gene expression and can be
235 used to prospectively identify peripheral $CD4^{+}$ T cells with elevated encephalitogenic properties.
236

237 **OCA-B promotes neuroinflammation in relapsing-remitting EAE models via control of**
238 **stem/memory-like T cell populations**
239 In contrast to the chronic form of EAE that develops in C57BL/6 mouse models, EAE on the NOD
240 background exhibits a relapsing-remitting pattern that more closely mimics human disease[40]. To
241 study the impact of OCA-B loss in T cells on mouse models that more closely resemble human
242 MS disease patterns, we utilized *Ocab* T cell conditional knockout mice crossed to the NOD
243 background[30]. EAE was induced in 15-18 week old female NOD.*Ocab*$^{fl/fl}$;CD4-Cre and littermate
244 control NOD.*Ocab*$^{fl/fl}$ mice with MOG_{35-55}. Clinical scores and weights were recorded for 47 days
245 to observe initial disease onset, relapse and relapse recovery. No significant differences in clinical
246 scores were observed between groups at disease onset (day 10-19), however following the
247 primary remission, NOD.*Ocab*$^{fl/fl}$;CD4-Cre animals were almost completely protected against
248 disease relapse (Fig. 5a). Individual NOD mouse clinical scores are shown in Extended Data Fig.
249 5a-b. Normalized weights of animals also reflected the protective effect of OCA-B loss in T cells
250 at relapse (Fig. 5b).
251 To understand differences in CNS-infiltrating T cells underlying relapse protection at a
252 population and transcriptional level, we performed single-cell RNA sequencing (scRNAseq) of
253 CD3ε^{+} T cell isolates from CNS (brain + spinal cord) at remission (day 24) and peak relapse (day
254 33). Cells from 3-6 NOD.*Ocab*$^{fl/fl}$;CD4-Cre and NOD.*Ocab*$^{fl/fl}$ littermate controls were collected and
255 combined for analysis. 7799 (remission) and 9224 (relapse) *Ocab* knockout, and 6009 (remission)
256 and 7525 (relapse) control cells were used for analysis, with an average per cell read depth
257 ranging from 90,000 to 190,000. For remission, Uniform Manifold Approximation and Projection
258 (UMAP) clustering using both genotypes revealed 16 clusters corresponding to a broad T cell
259 repertoire consisting of natural-killer T (NKT) cells (the largest cluster) and different CD4^{+} and
260 CD8^{+} subsets (Fig. 5c). Noteworthy clusters based on mRNA expression included proliferating
261 (*Ki67*, *Pcna*, *Mcm2*), Th1-like (*Tbx21*, *Ifng*, *Tnf*, *Il12rb2*) and Treg (*Foxp3*, *Ctla4*) (Supplementary
262 Table 3). Feature plots for *Foxp3* and *Mki67* are shown in Fig. 5d. Additional feature plots for
263 *Cxcr6*, *Il23r* and *Bach2* are shown in Extended Data Fig. 5c. Notably there was a large decrease
264 in NKT cell numbers in knockout mice (36% control vs. 14% experimental). Within this cluster,
265 changes in gene expression between control and conditional knockout groups were minimal. Most
266 NKT cells from both groups showed a limited inflammatory cytokine response, consistent with the
267 lack of clinical disease at remission (Extended Data Fig. 5d). The decrease in the large NKT
268 population in the experimental group proportionally increases the percentage contribution of the

269 other clusters, and therefore similar or decreased percentages of these cells identifies reduced
270 populations which correlate with protection from relapse, e.g. proliferating T cells. Other clusters
271 such as Tregs increased disproportionately. Differential gene expression analysis of key clusters
272 (Treg, Proliferating, and Th1-like) revealed increased expression of *Slamf6* in Tregs lacking OCA-
273 B, while OCA-B deficient proliferating and Th1-like cells showed decreased expression of genes
274 associated with quiescence (*Btg1* and *Samhd1*), memory/stemness (*Slamf6*, *Tcf7*, and *Sell*) and
275 pathogenicity (*Tcf7* and *Tox* co-expression, Fig. 5e). Spectral cytometry showed no significant
276 difference in the frequency of CNS infiltrating $CD4^+$ T cells between groups at remission (Fig. 5f).
277 However, OCA-B deficient $CD4^+$ T cells did show a significant reduction in CXCR6 and IFNγ/GM-
278 CSF co-expression, indicative of reduced Th17 pathogenicity (Fig. 5g-i). These results indicate
279 that loss of OCA-B in T cells selectively reduces proliferation and differentiation of pathogenic
280 stem/memory-like $CD4^+$ T cells during disease remission.

281 At relapse, multiple CNS-infiltrating stem-like and effector $CD4^+$ and $CD8^+$ control T cell
282 populations were present (Fig. 6a and Extended Data Fig. 6a; Supplementary Table 4). TCR
283 sequencing revealed an expansion of a subset of TCR clones in the OCA-B deficient CD8 clusters
284 while most other clusters were highly polyclonal (Fig. 6b). Comparing the 10 most expanded TCR
285 clonotypes between knockouts and controls, there were several clonotypes that were shared but
286 differentially expanded (Extended Data Fig. 6b and Supplementary Table 5). A "Ccr9 stem-like"
287 cluster expressing the gut homing chemokine receptor *Ccr9*, as well as *Ccr7*, *Bach2*, and *Tcf7*
288 notably appeared at relapse (Fig. 6c, Supplementary Table 4). TCR clonotype analysis indicated
289 that this population was highly polyclonal (Fig. 6b). Additionally, a "Stem-like CD4-2" cluster
290 expressing *Tcf7*, Ccr7, *Bach2, Cd44* and low-level *Cxcr6*, and a prominent "Th17-like" cluster
291 expressing *Tcf7, Cd44*, *Il1r1, Lgals3*, and higher levels of *Cxcr6* was identified (Fig. 6c). This latter
292 cluster likely contains pathogenic effector cells.

293 In the absence of OCA-B, NKT cell populations were normalized compared to the
294 remission timepoint, and several clusters showed major changes in the percentage of cells
295 including most prominently the Ccr9-stem-like cells which were much more prevalent (Fig. 6d).
296 Feature plots comparing OCA-B T cell deficient mice to littermate controls for *Ccr9* and the
297 transcription factors *Tcf7* and *Bach2* are shown in Fig. 6d. The cells were also marked by the
298 expression of *Cd4*, *Tox, Ccr7, Ccr4* and limited expression of *Sell* (Extended Data Fig. 6c).

299 RNA velocity analysis of spliced and unspliced transcripts[45] identified clusters of T cells,
300 most bearing static gene expression profiles consistent with terminal differentiation, but some with
301 differentiating or transitional gene expression (Fig. 6e). Notably, OCA-B knockout cells showed

302 increased transcriptional stasis within the Ccr9-stem-like and proliferating clusters, and a
303 decreased transcriptional directionality of Th17 cells towards gd17 cells, the latter of which
304 express high levels of pathogenic markers including *Il1r1*, *Cxcr6*, and *Lgals3* (Extended Data Fig.
305 6a). Pseudotime analysis identified a transcriptional capacity in the control *Ccr9* expressing
306 population to differentiate into pathogenic Th17-like cells, whereas cells lacking OCA-B were
307 limited in this capacity, possibly resulting in the accumulation of these cells (Extended Data Fig.
308 6d). These changes culminated in the Th17-like effector knockout cells expressing reduced
309 pathogenicity-associated genes such as *Pdcd1*, *Tigit* and *Il1r1* (Fig. 6f). Together these results
310 suggest OCA-B mediates the transition of non-pathogenic stem-like cells to pathogenic Th17 cells
311 which ultimately drive disease relapse.

312 **Discussion**

313 The development of therapies that inhibit autoimmunity while minimizing impacts on normal
314 immune function remains a critical unmet goal in the field. In this study, we show that expression
315 of the transcriptional co-regulator OCA-B promotes a pathogenic, stem/memory-like function in T
316 cells, resulting in the establishment of CNS autoimmunity, and in particular episodes of relapse.
317 Loss of OCA-B attenuates these populations in chronic EAE, in adoptive transfer EAE, and in
318 NOD.EAE during episodes of remission. During relapse, OCA-B T cell knockout mice are almost
319 completely protected, and accumulate a population of $CD4^+$ T cells expressing *Ccr9*, *Bach2*, and
320 *Tcf7*. OCA-B expression also marks viable pathogenic stem/memory-like $CD4^+$ T cells that
321 preferentially transfer EAE. Furthermore, the effects of modulating OCA-B are selective, as
322 responses to infection with a neurotropic coronavirus that generates similar clinical symptoms but
323 lacks an autoantigen were largely unaffected.

324 OCA-B is a member of a small family of transcription co-regulators that also includes OCA-
325 T1, OCA-T2 and IκBζ[46,47]. It docks with Oct1 upon $CD4^+$ T cell activation to directly regulate
326 immunomodulatory genes such as *Il2*, *Ifng*, *Il17a*, Tbx21 (T-bet) and *Csf2* (*Gmcsf*). Rather than
327 functioning as a primary inducer of these genes, it is required for their robust expression upon
328 antigen reencounter[20,30]. Notably, unlike transcription factors such as NF-AT, AP-1 and NF-κB,
329 Oct1 and OCA-B are dispensable for normal primary T cell responses[20]. These findings predict
330 important roles for OCA-B in $CD4^+$ T cells specifically in situations of antigen reencounter, which
331 is a necessary feature of autoimmunity. Conditional T cell knockout of Oct1 reduces EAE severity,
332 with reduced proinflammatory cytokine expression and increased anergy[21]. Deletion of Oct1 in T
333 cells was dispensable for neurotropic viral clearance[21], however the ubiquitous expression of Oct1
334 in adult tissue limits its translational potential. In contrast, OCA-B expression is largely confined
335 to B and T cells and whole-body knockout mice are viable and fertile[48]. OCA-B is highly expressed
336 in B cells and required for germinal center formation[49,50]. It is expressed in $CD4^+$ T cells upon
337 activation at levels 50-100-fold less than in B cells[30,51,52]. This suggests that with proper
338 therapeutic dosing, OCA-B could be inhibited selectively in T cells with minimal impact to the B
339 cell compartment. Short-term administration of an OCA-B peptide mimic that inhibits OCA-B's
340 downstream effector functions reverses spontaneous type-1 diabetes in NOD mice[30]. However,
341 toxicity limits its efficacy, including within EAE models. Further research is required for the
342 development of safe and effective OCA-B inhibitors.

343 OCA-B whole body knockout animals are partially protected from EAE[39], however, the
344 known activity of OCA-B in B cells made it unclear if the protection is T cell-derived. Here we
345 show that OCA-B promotes EAE pathogenesis through T cells. Opportunistic infections and
346 reactivation of latent CNS-tropic viruses are significant barriers for MS therapeutics that focus on
347 global immune suppression as a therapeutic mechanism. When OCA-B T cell conditional
348 knockout mice are challenged with the neurotropic coronavirus JHMV, there is little difference in
349 their ability to mount immune responses and control virus replication. This finding provides a
350 potential therapeutic window in which targeting the low levels of OCA-B in T cells could be used
351 to blunt autoimmunity while sparing baseline immune responses.
352 Unlike the significant but modest protection observed in chronic C57BL/6 EAE, OCA-B
353 loss in adoptive transfer EAE almost completely protects recipient animals from disease. This
354 may indicate that adoptive transfer EAE models involve more autoantigen re-exposures, as
355 transferred T cells must re-encounter antigen in a naïve host before promoting disease. Protection
356 was observed regardless of whether donor cells were Th1- or Th17-polarized, indicating that
357 OCA-B functions through a mechanism that parallels rather than enforces the Th1/Th17
358 paradigm. We therefore sought other mechanisms that might explain why OCA-B T cell knockouts
359 are so strongly protected.
360 Recent findings indicate an emerging role for stem/memory-like T cells in promoting
361 autoimmunity[44,53]. For example, myelin-specific $CD4^+$ T cells in MS patients show signs of a
362 previously activated, memory-like phenotype compared to healthy controls[9,10,12]. Furthermore,
363 memory-like Th1 and Th17 cells are increased in the peripheral blood of MS patients and display
364 increased pathogenicity compared to conventional Th17 Cells[54]. Similarly, in EAE models,
365 peripheral central memory-like $CD4^+CD44^{hi}CD62L^{hi}$ T cells confer increased disease severity
366 upon transfer[14]. Both Oct1 and OCA-B promote the functionality of long-lived $CD4^+$ memory T
367 cells following antigenic rechallenge[29,55]. An OCA-B-mCherry reporter mouse allele, which
368 effectively labels memory progenitor $CD4^+$ T cells during acute infection[29], also labels $CD4^+$ T
369 cells that preferentially confer EAE. OCA-B^{hi} cells taken from the CNS at peak EAE selectively
370 express stem/memory markers. Further profiling OCA-B^{hi} $CD4^+$ T cells suggests that OCA-B
371 promotes the transition of non-pathogenic stem-like cells to a pathogenic state associated with
372 markers such as *Cxcr6*, *Slamf6*, *Ifng*, and *Il17a*. The connection between OCA-B expression and
373 pathogenic memory/stem-like T cells likely has not been appreciated before because OCA-B is
374 expressed at levels too low to be reproducibly captured with many current single-cell RNA-seq
375 technologies.

376 Relapsing-remitting EAE models have been developed using the Swiss Jim Lambert (SJL)
377 and autoimmune prone non-obese diabetic (NOD) backgrounds[40,56]. In NOD mice, MOG_{35-55} EAE
378 has been described as relapsing-remitting with minimal initial disease that increases in severity
379 upon relapse[57,58]. Using this model with the conditional *Pou2af1* allele backcrossed to the NOD
380 background[30], we found that OCA-B T cell loss minimally affects initial clinical presentation, but
381 instead protects animals specifically at relapse. The finding that OCA-B loss in conventional
382 C57BL/6 EAE results in partial protection intermediate between the initial and relapse phases of
383 NOD.EAE suggests that chronic C57BL/6 EAE may not model either initial presentation or relapse
384 accurately, but instead represents a superposition of the two.
385 Single-cell RNA expression profiling at remission identifies a significant loss of *Slamf6*,
386 *Tcf7* (encoding TCF1) and *Sell* from proliferative stem-like $CD4^+$ T cells in the OCA-B deficient
387 condition. While the majority of research on TCF1-expressing stem-like T cells focuses on $CD8^+$
388 populations with the capacity for self-renewal and differentiation into effector cells, analogous
389 descriptions have been made for $CD4^+$ populations[44,59,60]. Indeed, autoimmune $CD4^+$ T cells
390 expressing these memory/stem-like markers have been reported as an encephalitogenic
391 reservoir that play a key role in EAE pathogenicity[44]. In the same study, bulk RNA sequencing
392 associated OCA-B expression within this stem-like reservoir[44].
393 Single-cell RNA-seq at relapse identified multiple emergent populations of effector T cells
394 compared to remission. Notably, there was also an accumulation of a unique population of $CD4^+$
395 cells in OCA-B T cell deficient mice. These cells are conspicuously marked by expression not
396 only of *Ccr4*, but also of *Ccr9*, which encodes a gut-homing chemokine receptor. $CCR9^+$ memory-
397 like $CD4^+$ T cells have been linked to MS and EAE protection[61]. The cells also express *Bach2*, a
398 transcription regulator which was recently associated with non-pathogenic immunomodulatory
399 Th17-polarized cells in the context of C57BL/6 EAE[62]. *Bach2* expression was largely concentrated
400 in the "CCR9 stem-like" cluster, which is more numerous in the knockout condition. Consistently,
401 in bulk RNA-seq *Bach2* mRNA was upregulated in OCA-B^- cells ($p<10^{-13}$), although with a small
402 (+1.74) fold change (Supplementary Table 1). In B cells, OCA-B is known to regulate *Bach2*[63].
403 Velocity and pseudotime analysis indicates that these cells are normally transcriptionally inclined
404 to progress towards an highly pathogenic Th17 population, but that progression stalls in mice
405 whose T cells lack OCA-B. Consistently, the Th17 effector population in OCA-B T cell knockout
406 mice lacks expression of key genes such as *Il1r1* and *Pdcd1*, both of which are associated with
407 pathogenicity in CNS-infiltrating Th17 cells[48,64]. The cumulative alterations in these populations in
408 OCA-B knockouts likely explains why these mice are strongly protected against disease relapse.

409 In conclusion, this study indicates a prominent role for OCA-B in driving stem-like $CD4^+$ T cell
410 populations towards a pathogenic state while playing a minimal role in acute antiviral responses
411 to a CNS infection.

412 **Figure legends**

413 **Fig.1 I OCA-B loss protects animals from chronic EAE**

414 **a**, *Ocab*$^{fl/fl}$ (n=16) and *Ocab*$^{fl/fl}$;CD4-Cre (n=22) mice were injected with MOG$_{35-55}$ peptide in CFA
415 and *pertussis* toxin to induce EAE. Clinical scores were evaluated after EAE induction to
416 determine disease progression. **b**, Animal weights were recorded to evaluate weight loss as a
417 measurement of disease progression. **c**, Representative DAPI/MBP immunostaining of thoracic
418 sections taken from mice 15 days after EAE induction. Areas of demyelination are marked by
419 decreased MBP staining (green) and often coincide with increased cellular infiltration (blue). **d**,
420 Quantification of demyelination in experimental (n=6) and control mice (n=5). **e**, Brain and spinal
421 cords were isolated on day 15 of EAE and analyzed by spectral cytometry. Representative flow
422 cytometry plots of CD45$^+$TCRβ$^+$ CNS infiltrating T cells showing frequency of CD4$^+$ and CD8$^+$ T
423 cells. **f**, Quantification of the number of CNS infiltrating CD4$^+$ T cells. *Ocab*$^{fl/fl}$ (n=13) and
424 *Ocab*$^{fl/fl}$;CD4-Cre (n=9). **g**, Representative plots showing frequency of CD44$^+$ MOG$_{38-49}$ tetramer-
425 positive CD4$^+$ T cells. **h**, Quantification of the frequency and count of CD44$^+$ MOG$_{38-49}$ tetramer-
426 positive CD4$^+$ T cells. *Ocab*$^{fl/fl}$ (n=12) and *Ocab*$^{fl/fl}$;CD4-Cre (n=9). For clinical scores and
427 normalized weights, data represent mean ±SEM. All other data represents mean ±SD.

428

429 **Fig.2 I OCA-B promotes Th1 and Th17 adoptive transfer EAE through recall response**

430 **a**,**b**, *Ocab*$^{fl/fl}$ and *Ocab*$^{fl/fl}$;CD4-Cre mice were primed with MOG$_{35-55}$ peptide in CFA for 10-14 days.
431 Cells from the spleens and lymph nodes of primed mice were isolated and cultured for 4 days in
432 Th1 or Th17 polarizing conditions. 3.0x10^6 Th1- or Th17-polarized cells were injected i.p. into
433 C57BL/6 wildtype recipient mice (Th1: *Ocab*$^{fl/fl}$ n=5, *Ocab*$^{fl/fl}$;CD4-Cre n=5) (Th17: *Ocab*$^{fl/fl}$ n=3,
434 *Ocab*$^{fl/fl}$;CD4-Cre n=4). Clinical scores were assessed for 14-15 days. **c**, At Th17 adoptive transfer
435 EAE endpoint, brains and spinal cords were analyzed by flow cytometry. Quantification of brain-
436 and spinal cord-infiltrating CD4$^+$ T cells following Th17 adoptive transfer. **d**, Representative flow
437 cytometry plots showing the frequency of IFNγ and IL-17 expressing CD4$^+$ T cells within the spines
438 of Th17 recipient mice. **e**, Quantification of IL-17 frequency in spinal cord infiltrating CD4$^+$ T cells.
439 **f**, Quantification of the total count of IL-17$^+$ CD4$^+$ T cells within the spinal cord of recipient mice.
440 For clinical scores, data represent mean ±SEM. All other data represents mean ±SD.

441

442

443 **Fig.3 I OCA-B is dispensable for T cell response to CNS infection with a neurotropic virus**

444 **a**, *Ocab*$^{fl/fl}$ (n=19) and *Ocab*$^{fl/fl}$;CD4-Cre (n=17) mice were injected intracranially with 1500 PFU
445 JHMV. Clinical scores were recorded for 21 days post infection (dpi). **b**, Representative
446 DAPI/MBP immunofluorescence staining of spinal cord sections at 12 dpi. Demyelinated areas
447 are marked by decreased MBP staining (green) and often coincide with increased cellular
448 infiltration (blue). **c**, Quantification of % demyelination in spinal cord sections. (n=7 per group).
449 Half brains were taken at 7, 12, and 21 dpi for flow cytometric and viral titer analysis. **d**,
450 Quantification of CD4$^+$ T cell counts within half brain at 7, 12, 21 dpi. *Ocab*$^{fl/fl}$ (n=7-9 per time
451 point) and *Ocab*$^{fl/fl}$;CD4-Cre (n=6-7 per time point). **e**, Representative plots showing the frequency
452 of IFNγ expressing CD4$^+$ T cells 7, 12, and 21 dpi. **f**, Quantification of frequency of IFNγ expressing
453 CD4$^+$ T cells. *Ocab*$^{fl/fl}$ (n=7-9 per time point) and *Ocab*$^{fl/fl}$;CD4-Cre (n=6-7 per time point). **g**, Half
454 brain viral titers at dpi 7, 12, and 21 (n.d., not detected). *Ocab*$^{fl/fl}$ (n=7-9 per time point) and
455 *Ocab*$^{fl/fl}$;CD4-Cre (n=6-7 per time point). These data represent the combined results of two
456 independent experiments. For clinical scores, data represent mean ±SEM. All other data
457 represents mean ±SD.
458
459 **Fig.4 | OCA-B expression marks encephalitogenic stem-like CD4$^+$ T cells**
460 **a**, OCA-B-mCherry mice were injected with MOG$_{35-55}$ peptide in CFA and *pertussis* toxin to induce
461 EAE. Cervical lymph nodes (CLNs), brains, and spines were isolated at peak disease (day 15)
462 and analyzed by flow cytometry for mCherry, CD44 and CD62L expression. **b**, CD44 and CD62L
463 expressing CD4$^+$ T cells were quantified based on mCherry expression. **c**, OCA-B-mCherry mice
464 were injected with MOG$_{35-55}$ peptide in CFA for 14 days. CD4$^+$ T cells within CLNs and spleens
465 were profiled by flow cytometry for mCherry, CD44, and CD62L expression. **d**, Quantification of
466 CD44 and CD62L expression of OCA-B negative and positive CD4$^+$ T cells from MOG-primed
467 OCA-B-mCherry mice. **e**, Bulk RNA sequencing was performed on OCA-B positive and negative
468 CD4$^+$ T cells from MOG$_{35-55}$ primed OCA-B-mCherry reporter mice. Heatmap showing relative
469 expression of the top 40 differentially expressed genes from OCA-B positive and negative CD4$^+$
470 T cells. **f**, Volcano plot of differentially expressed genes between OCA-B positive and negative T
471 cells (p value > 0.05 and Log2 fold change > 1 are colored). **g**, Gene Ontology (GO) terms
472 associated with OCA-B positive and negative groups. **h**, EAE clinical scores of C57BL/6 wild-type
473 mice following passive transfer of OCA-B-positive or -negative Th1 polarized CD4$^+$ T cells. Clinical
474 score values represent mean ±SEM. All other data represent mean ±SD.
475

476 **Fig.5 I OCA-B promotes relapsing-remitting EAE through stem-like CD4$^+$ T cells**

477 **a**, NOD.*Ocab*$^{fl/fl}$ (n=19) and NOD.*Ocab*$^{fl/fl}$;CD4-Cre (n=15) mice were injected with MOG$_{35-55}$
478 peptide in CFA and *pertussis* toxin to induce EAE. Clinical scores of animals representing
479 relapsing-remitting disease progression over time. **b**, Animal weights were recorded to determine
480 weight loss throughout initial disease and relapse. **c**, Singe cell RNA sequencing was performed
481 on pooled CD3ε$^+$ cells isolated from the brain and spine of NOD.*Ocab*$^{fl/fl}$ (n=3) and
482 NOD.*Ocab*$^{fl/fl}$;CD4-Cre (n=4) 24 days after EAE induction (remission timepoint). Cell populations
483 were plotted in a UMAP using the Seurat R package and percentages are shown for each cluster.
484 Clusters were identified through differential gene expression analysis. **d**, Feature plots comparing
485 the expression of *Foxp3* and *Mki67* amongst clusters. **E,** Violin plots showing the expression of
486 *Btg1*, *Samhd1*, *Slamf6*, *Tcf7, Sell* and *Tox* within the Treg, proliferating, and Th1-like clusters. **f**,
487 CNS cells isolated at remission timepoint (day 24) were analyzed by spectral cytometry.
488 Representative flow cytometry plots and quantification showing the frequency of CD4$^+$ T cells
489 between control and experimental groups. **g**, Representative flow cytometry plots and
490 quantification showing the frequency of CXCR6 expressing CD4$^+$ T cells. **h,** Representative flow
491 cytometry plots showing the frequency of CD4$^+$ T cells expressing IFNγ and GM-CSF. **i**,
492 Quantification of CD4$^+$ T cells expressing IFNγ and GM-CSF. For clinical scores, data represents
493 mean ±SEM. All other data represents mean ±SD.

494

495 **Fig.6 I OCA-B promotes disease relapse through control of pathogenic stem-like Th17**
496 **differentiation**

497 **a**, Singe cell RNA and TCR sequencing were performed on pooled CD3ε$^+$ cells isolated from the
498 brain and spine of NOD.*Ocab*$^{fl/fl}$ (n=5) and NOD.*Ocab*$^{fl/fl}$;CD4-Cre (n=6) 33 days after EAE
499 induction (relapse timepoint). Cell populations were plotted in a UMAP using the Seurat R
500 package and percentages are shown for each cluster. Clusters were identified through differential
501 gene expression analysis. **b**, UMAP TCR clonotype expansion between *Ocab*$^{fl/fl}$ and *Ocab*$^{fl/fl}$;CD4-
502 Cre amongst clusters. **c**, Violin plots showing expression of *Ccr9*, *Bach2*, *Ccr7*, *Tcf7*, *Cd44*, *Cxcr6*,
503 *Il1r1* and *Lgals3* in the Ccr9 Stem-like CD4, Stem-like CD4-2, and Th17-like clusters. **d**, Feature
504 plots comparing the expression of *Ccr9*, *Tcf7*, and *Bach2* amongst clusters. **e**, UMAPs showing
505 RNA velocity of spliced and unspliced transcripts by experimental condition. **f**, Violin plots showing
506 expression of *Pdcd1*, *Tigit*, and *Il1r1* in the Th17-like cluster between control and experimental
507 groups.

508 **Extended data legends**

509 **Extended Data Fig.1. Minimal differences in cytokine expressing CD4$^+$ T cell, CD8$^+$ T cell,**
510 **B cell, macrophage or microglial cell counts at peak chronic EAE in OCA-B knockouts**

511 **a**, Representative spinal cord LFB/H&E staining of thoracic sections taken from mice 15 days
512 after EAE induction. Areas of demyelination are outlined in black and marked by increased loss
513 of LFB (blue) staining and visibility of H&E (pink) within the white matter. **b**, Quantification of the
514 % demyelination from LFB/H&E histology. **c**, Quantification of the frequency of CNS infiltrating
515 CD4$^+$ T cells between Ocab$^{fl/fl}$ and Ocab$^{fl/fl}$;CD4-Cre mice. **d**, Quantification of frequency and count
516 of CD8α positive T cells between Ocab$^{fl/fl}$ and Ocab$^{fl/fl}$;CD4-Cre mice. **e**, Quantification of the
517 number of B cells, macrophages and microglia. **f**, Representative flow cytometry plots comparing
518 the expression of CD44$^+$ within CNS infiltrating CD8$^+$ T cells from Ocab$^{fl/fl}$ and Ocab$^{fl/fl}$;CD4-Cre
519 mice. **g**, Quantification of the frequency of CNS infiltrating CD44$^+$ CD8$^+$ T cells within Ocab$^{fl/fl}$ and
520 Ocab$^{fl/fl}$;CD4-Cre mice. **h**, Quantification of frequency and count of IFNγ, IL-17, GM-CSF, and
521 CD44 expressing CD4$^+$ T cells from Ocab$^{fl/fl}$ and Ocab$^{fl/fl}$;CD4-Cre mice. All data represents mean
522 $\pm$SD.

523

524 **Extended Data Fig.2. Loss of OCA-B does not strongly alter initial Th1 or Th17 polarization**
525 **in vitro**

526 **a**, Experimental schematic for assessing CD4$^+$ T cell differences between Ocab$^{fl/fl}$ and
527 Ocab$^{fl/fl}$CD4-Cre prior to *in vitro* Th1 or Th17 polarization. Lymph nodes (cervical, brachial,
528 axillary, and inguinal) were harvested from Ocab$^{fl/fl}$ (n=4) and Ocab$^{fl/fl}$;CD4-Cre (n=4) mice
529 following 14 days of MOG$_{35-55}$/CFA priming and analyzed by flow cytometry **b**, Frequency of
530 viable cells isolated from Ocab$^{fl/fl}$ and Ocab$^{fl/fl}$;CD4-Cre mice. **c**, Total CD4$^+$ T cell numbers
531 isolated from Ocab$^{fl/fl}$ and Ocab$^{fl/fl}$;CD4-Cre mice. **d**, Quantification of the frequency of IFNγ
532 expressing CD4$^+$ T cells isolated from Ocab$^{fl/fl}$ and Ocab$^{fl/fl}$;CD4-Cre mice. **e**, Quantification of
533 the frequency of IL-17 expressing CD4$^+$ T cells derived from Ocab$^{fl/fl}$ and Ocab$^{fl/fl}$;CD4-Cre mice.
534 **f**, Frequency of Ki67 expressing CD4$^+$ T cells from Ocab$^{fl/fl}$ and Ocab$^{fl/fl}$;CD4-Cre mice. CD4$^+$ T
535 cells were isolated from Ocab$^{fl/fl}$ (n=8) and Ocab$^{fl/fl}$;CD4-Cre (n=8) mice following 14 days of
536 MOG$_{35-55}$/CFA priming, fluorescently labeled using QTracker nanocrystals (Ocab$^{fl/fl}$-QTracker
537 655) (Ocab$^{fl/fl}$;CD4-Cre-Qtracker 525), injected i.p. into naïve C57BL/6 recipients and assessed
538 after 3 days by flow cytometry. **g**, Representative flow cytometry plot showing QTracker 655 and
539 QTracker 525 labeled CD4$^+$ T cells isolated from the peritoneal cavity of recipient mice. **h**,

540 Quantification of the frequency of QTracker 655 and QTracker 525 labeled $CD4^+$ T cells isolated
541 from the peritoneal cavity of recipient mice. **i**, Representative flow cytometry plots comparing
542 viability of peritoneal QTracker 655 and QTracker 525 labeled $CD4^+$ T cells by Live/Dead Blue
543 staining. **j**, Peritoneal QTracker 655 and QTracker 525 labeled $CD4^+$ T cell viability
544 quantification. **k**, Representative flow cytometry plots showing Ki67 expression within QTracker
545 655 and QTracker 525 labeled $CD4^+$ T cells isolated from the peritoneal cavity. **l**, Quantification
546 of the frequency of Ki67 expressing QTracker 655 and QTracker 525 labeled $CD4^+$ T cells. **m**,
547 Representative flow cytometry plots showing IFNγ and IL-17 expressing $CD4^+$ T cells from
548 $Ocab^{fl/fl}$ (n=5) and $Ocab^{fl/fl}$;CD4-Cre (n=5) mice after Th1 and Th17 *in vitro* polarization. **n**,
549 Quantification of IFNγ expressing $CD4^+$ T cells after Th1 polarization. **o**, Quantification of IL-17
550 expressing $CD4^+$ T cells after Th17 polarization. **p**, Quantification of the frequency of IFNγ
551 expressing $CD4^+$ T cells isolated from the spinal cords of Th17 adoptive transfer EAE recipient
552 mice. All data represents mean ±SD.
553
554 **Extended Data Fig.3. Normal immune responses to intracranial JHMV infection in the**
555 **absence of OCA-B**
556 **a**, Representative LFB/H&E histology of spinal cord sections at dpi 21. **b**, Demyelination
557 quantification of LFB/H&E histology at dpi 21. **c**, Quantification of the number of IFNγ expressing
558 $CD4^+$ T cells at dpi 7, 12 and 21. **d**, Quantification of the number of $CD8^+$ T cells at dpi 7, 12 and
559 21. **e**, Quantification of the frequency of IFNγ expressing $CD8^+$ T cells at dpi 7, 12 and 21. **f,**
560 Quantification of the number of IFNγ expressing $CD8^+$ T cells at dpi 7, 12 and 21. All data
561 represents mean ±SD.
562
563 **Extended Data Fig.4. Sorting OCA-B-mCherry reporter T cells and additional analysis of**
564 **the effects of transferring OCA-B^{hi} versus OCA-B^{lo} $CD4^+$ cells**
565 **a**, Quantification of the frequency of $CD44^+$ $CD62^-$ $CD4^+$ T cells within the cervical lymph nodes
566 of OCA-B-mCherry reporter mice at peak EAE by OCA-B-mCherry expression. **b**, Gating
567 strategy for sorting of OCA-B^+ and OCA-B^- $CD4^+$ T cells. **c**, Normalized weights of NOD.$Ocab^{fl/fl}$
568 and NOD.$Ocab^{fl/fl}$;CD4-Cre mice following EAE induction. Normalized weight is represented by
569 mean ±SEM. All other data represents mean ±SD.
570

571 **Extended Data Fig.5. Individual NOD mouse EAE clinical scores, additional remission**
572 **scRNA-seq cluster annotation genes, and heat map of gene enrichments by cluster**
573 **a**, Clinical scores of individual NOD.Ocab$^{fl/fl}$ mice following EAE induction. **b**, Clinical scores of
574 individual NOD.Ocab$^{fl/fl}$;CD4-Cre mice following EAE induction. **c**, UMAP feature plots showing
575 expression of *Cxcr6*, *Il23r*, and *Bach2* amongst clusters at remission timepoint. **d**, Heatmap
576 showing the top 10 genes expressed by cluster at remission EAE timepoint.
577
578 **Extended Data Fig.6. Heat map of NOD.EAE relapse gene enrichments by cluster, TCR**
579 **clonotype overlap between condition, example relapse feature plots, and pseudotime**
580 **analysis of relapse single cell RNA seq**
581 **a**, Heatmap showing the top 10 genes expressed by cluster at relapse EAE timepoint. **b,** Alluvial
582 plot showing top 10 TCR clonotype gene overlap between Ocab$^{fl/fl}$ and Ocab$^{fl/fl}$;CD4-Cre groups.
583 **c**, UMAP feature showing the expression of *CD4*, *CD8a, Tox*, *Sell*, *Ccr7*, and *Ccr4* amongst
584 clusters at relapse timepoint. **d**, Pseudotime analysis of relapse single cell from root starting
585 node at or near Ccr9 stem-like cluster.
586
587 **Extended Data Fig.7. OCA-B promotes pathogenic maturation of stem-like Th17 cells in**
588 **EAE**
589 OCA-B expression promotes and selectively labels pathogenic stem-like Th17 cells which
590 preferentially transfer EAE and instigate disease relapse.

591 **Methods**

592 **Chronic C57BL/6 EAE**

593 All animal work was approved by the University of Utah Institutional Animal Care and Use
594 Committee. 11-12 week-old female C57BL/6 littermate animals were used for all experiments.
595 For adoptive transfer experiments using the OCA-B-mCherry reporter allele[29], 11 week-old
596 females were used for chronic EAE and 9 week-old males were used as MOG_{35-55} primed adoptive
597 transfer donors. EAE was induced on day 0 by two 100 μL s.c. injections into both hind flanks of
598 0.5 μmol/mL MOG_{35-55} peptide (University of Utah Peptide Core) emulsified in complete Freud's
599 adjuvant (CFA), comprised of incomplete Freund's adjuvant (Cat# 77145;ThermoFisher) together
600 with 4 mg/mL heat-killed *M. tuberculosis* (Cat# DF3114338; Fisher Scientific). Animals were given
601 two 400 ng i.p. injections of *B. pertussis* toxin (Cat# 181; List Biological Laboratories) on days 0
602 and 2.

603

604 **Clinical Scoring**

605 EAE clinical scores were determined using a 0-5 scale with 0.5 scoring intervals: 0.5, tip of tail is
606 limp or tail muscle strain observed; 1, complete limp tail; 1.5, complete limp tail and at least one
607 hind limb consistently falls through wire rack when animal is dropped; 2, complete limp tail and
608 one hind leg dragging without movement beyond hip; 2.5, complete limp tail and dragging of both
609 hind limbs without movement beyond hip; 3, complete hind limb paralysis; 3.5, complete hind limb
610 paralysis with flat laying hind quarters and hump in upper torso; 4, complete hind limb and partial
611 forelimb paralysis, minimal movement around cage; 4.5, complete hind limb and partial forelimb
612 paralysis, no movement around cage; 5, seizure or death. Animals scoring a ≥4 for more than 48
613 hours were euthanized and scored 5 for the remainder of the experiment. JHMV clinical disease
614 was evaluated using previously described 0-4 point scale[65].

615

616 **Immunofluorescence and Histology**

617 Spinal columns were isolated from C57BL/6 $Ocab^{fl/fl}$ and $Ocab^{fl/fl}$;CD4-Cre animals after EAE or
618 JHMV induced demyelination and fixed overnight in in 4% paraformaldehyde at 4C. Spinal cords
619 were subsequently isolated and cryoprotected in 30% sucrose for 3-5 days. Thoracic and lumbar
620 sections were embedded in optimum cutting temperature (OCT) compound (ThermoFisher
621 Scientific) and frozen and stored at -80C. 8 µm spinal sections were cut by cryostat and stained
622 with Luxol fast blue (Cat# 212170250; ThermoFisher) along with hematoxylin (Cat# 8495; ENG

623 Scientific) and eosin (Cat# E511-25; Fisher Chemical). Demyelination was assessed by dividing
624 the area of demyelinated white matter by total white matter as previously described[66,67]. For
625 immunofluorescence, spinal cord sections were blocked in 5% normal goat serum (NGS; Cat#
626 005-000-121, Jackson ImmunoResearch) and 0.1% Tween-20 for 1 hour at room temperature.
627 Sections were stained overnight at 4°C with primary antibody rabbit anti-MBP (1:1000; Cat#
628 PA1050, Boster), followed by secondary antibody goat anti-rabbit conjugated with Alexa Fluor
629 488 (1:750; Cat# A11008, Invitrogen) for 2 hours at room temperature. Primary and secondary
630 antibodies were diluted in 1% bovine serum albumin (BSA) and 0.1% Tween-20. Slides were
631 cover-slipped using Fluoromount-G with DAPI (Cat# 00495952, Invitrogen). Sections were
632 imaged with a Zeiss Axioscan 7 Microscope Slide Scanner using a 20× objective.
633
634 **Flow cytometry and spectral cytometry**
635 Spinal cords and brains were harvested at peak disease or specified timepoint and mechanically
636 dissociated by passing through a 100 µm cell strainer. A 30/70% Percoll gradient (Cat# 17544501;
637 Cytiva) was used to enrich mononuclear cells. Cells from collected spleens and lymph nodes
638 (cervical, brachial, axillary and inguinal) were passed through a 70 µm strainer and erythrocytes
639 lysed by ammonium-chloride-potassium lysis buffer (150 mM NH_4Cl, 10 mM $KHCO_3$, 0.1 mM
640 Na_2EDTA). For intracellular staining, cells were cultured in complete media (RPMI 1640, 10%
641 FBS, 1% Pen/Strep, Glutamax) supplemented with 1 µL/mL brefeldin A (Cat# 555029; Golgiplug,
642 BD), 50 ng/mL phorbol myristate acetate (Cat# P1585; Sigma-Aldrich) and 1 µg/mL ionomycin
643 (Cat# I0634; Sigma-Aldrich) for 4 hr. Cultured cells were fixed using cytofix/cytoperm (Cat#
644 554714; BD) according to manufacturer's protocol and stained for intracellular cytokines in
645 perm/wash buffer. Flow cytometry samples were profiled using a BD Fortessa (BD Biosciences,
646 Fig. 2, 3, 4) or an Aurora spectral flow cytometer (Cytek, Fig. 1, 2, 5). FlowJo software (BD
647 Biosciences) was used for data analysis.
648
649 **Th1 and Th17 polarization and adoptive transfer C57BL/6 EAE**
650 10-12 week-old female C57BL/6 littermate animals were used for all experiments. Donor animals
651 were immunized with MOG_{35-55} in CFA as above. 10-14 days post-immunization, spleen and
652 lymph node (cervical, axillary, brachial and inguinal) cells were collected and placed into mixed
653 culture with MOG peptide and cytokines at 5.0×10^6 cells/mL. For Th1 conditions, complete media
654 was supplemented with 50 µg/mL MOG_{35-55}, 6 ng/mL rmIL-6 (Cat# 216-16; Peprotech) and 2

655 ng/mL rmIFNγ (Cat# 315-05; Peprotech). For Th17 conditions, complete media was
656 supplemented with 50 μg/mL MOG_{35-55}, 8 ng/mL rmIL-23 (Cat# 1887-ML-010; R&D Systems), 10
657 ng/mL rmIL-1α (Cat# 211-11A; Peprotech), and 10 μg/mL anti-IFNγ (Cat# BE0055; BioXcell
658 XMG1.2). After 4 days of respective culture, $CD4^+$ T cells were purified using negative magnetic
659 selection and resuspended in PBS at 1.5×10^6 cells/mL. 100 μL cell suspension was injected i.p.
660 into age-matched male C57BL/6 recipients (~13 week-old at time of disease induction). Clinical
661 disease was scored for 15 days.
662
663 **Pre-polarization profiling and mixed adoptive transfer**
664 10 week-old C57BL/6 *Ocab*$^{fl/fl}$ and *Ocab*$^{fl/fl}$*;CD4-Cre* littermates were immunized with MOG_{35-55} in
665 CFA as described above. After 14 days, spleen and lymph node (cervical, axillary, brachial and
666 inguinal) cells were isolated as described above. For the pre-polarization analysis (Extended Data
667 Fig. 2b-f), isolated lymph node cells were cultured in complete media (RPMI 1640, 10% FBS, 1%
668 Pen/Strep, Glutamax) supplemented with 1 μL/mL brefeldin A (Cat# 555029; Golgiplug, BD), 50
669 ng/mL phorbol myristate acetate (Cat# P1585; Sigma-Aldrich) and 1 μg/mL ionomycin (Cat#
670 I0634; Sigma-Aldrich) for 4 hr. Cells were stained for surface markers, fixed using the
671 Foxp3/Transcription Factor Staining Buffer Kit (Cat#00-5523-00, ThermoFisher), and stained for
672 intracellular markers (IFNγ, IL-17, and Ki67). For the mixed adoptive transfer (Extended Data Fig.
673 2g-l), $CD4^+$ cells were enriched from isolated splenocytes by magnetic negative selection (Miltenyi
674 Bio kit and LS columns). Enriched $CD4^+$ T cells from *Ocab*$^{fl/fl}$ donors were labeled with QTracker
675 655 (Cat#Q25021MP, ThermoFisher) and enriched $CD4^+$ T cells from *Ocab*$^{fl/fl}$*;CD4-Cre* donors
676 were labeled with QTracker 525 (Cat#Q25041MP, ThermoFisher) according to manufactures
677 instructions. Labeled cells from both genotypes were mixed at a 1:1 ratio and injected i.p. into
678 naïve age-match C56BL/6 recipients at 6.0×10^6 cells per mouse. After 72 hours, cells were
679 isolated from the peritoneal cavity of mixed adoptive transfer recipients as previously described[68].
680 Isolated cells were stimulated in the presence of brefeldin A, fixed and stained for surface and
681 intracellular markers as described above. Cells were analyzed by spectral cytometry for presence
682 of QTracker nanocrystals, viability by Live/Dead Blue staining (Cat#L23105, ThermoFisher) and
683 Ki67 expression.
684
685 **JHMV**

686 *Ocab*$^{fl/fl}$ and *Ocab*$^{fl/fl}$;CD4-Cre C57BL/6 mice were anesthetized using isoflurane. Mice were
687 intracranially (i.c) injected with 1500 plaque-forming units (PFU) of JHMV (strain V34) suspended
688 in 30 µL Hank's balanced salt solution (ThermoFisher). Clinical disease was assessed for 21 days
689 using a previously described scale[69]. Mice were sacrificed at days 7, 12, and 21 post-infection to
690 assess viral titers within brain homogenates using a plaque assay previously described[70]. Spinal
691 cords were taken on day 12 and 21 post-infection to assess demyelination by DAPI/MBP and
692 luxol fast blue and hematoxylin/eosin histology respectively.
693
694 **OCA-B-mCherry adoptive transfer EAE**
695 OCA-B-mCherry reporter allele animals[29] were primed for 14 days with MOG_{35-55} in CFA as
696 described above. After priming, spleen and lymph nodes were collected and $CD4^+$ T cells were
697 purified by magnetic negative selection (Miltenyi Bio kit and LS columns). Non-$CD4^+$ T cells were
698 removed from the LS column and placed on ice for subsequent in vitro culture. Purified $CD4^+$ T
699 cells were separated by OCA-B-mCherry expression (PE-Texas Red) using flow automated cell
700 sorting (FACS). OCA-B-mCherry positive and negative $CD4^+$ T cells were placed into mixed
701 culture in complete medium with the previously purified non-$CD4^+$ T cells at a 1:10 ratio ($CD4^+$ to
702 non-$CD4^+$) at 1.0×10^6 cells/mL. The culture was supplemented with 20 µg/mL MOG_{35-55} and 0.5
703 ng/mL IL-12p70 (Cat# 210-12; Peprotech). After two days of culture, $CD4^+$ T cells were again
704 purified through negative magnetic selection. Purified $CD4^+$ T cells from OCA-B-mCherry positive
705 and negative cultures were resuspended in PBS at 8.8×10^6 cells/mL. 100 µL cell suspension was
706 injected i.p. into age-matched male C57BL/6 recipients. Clinical disease was assessed for 24
707 days.
708
709 **Bulk RNAseq**
710 OCA-B-mCherry reporter mice (n=9) were primed for 14 days with MOG_{35-55} in CFA as described
711 above. After priming, lymph nodes (cervical, axillary, brachial and inguinal) were isolated and
712 mCherry positive and negative $CD4^+$ T cells were collected by FACS. Total RNA, three groups
713 (pooled 3 mice each), was isolated using the Quick RNA micro kit (Cat# R1050; Zymo Research)
714 with DNase treatment (Cat# 79254; Qiagen). RNA concentration was measured with a Qubit RNA
715 HS Assay Kit (Cat# #Q32855; Fisher Scientific). RNA quality was evaluated with an RNA
716 ScreenTape Assay (Cat# 5067-5579, 5067-5580; Agilent Technologies). Total RNA samples (5-
717 500 ng) were hybridized with NEBNext rRNA Depletion Kit v2 (Cat# E7400; New England Biolabs)

718 to diminish rRNA from the samples. Stranded RNA sequencing libraries were prepared as
719 described using the NEBNext Ultra II Directional RNA Library Prep Kit for Illumina (Cat# E7760L;
720 New England Biolabs). Purified libraries were qualified on an 4150 TapeStation (Agilent
721 Technologies) using a D1000 ScreenTape assay (Cat# 5567-5582, 5067-5583; Agilent
722 Technologies). The molarity of adapter-modified molecules was defined by quantitative PCR
723 using the Kapa Biosystems Kapa Library Quant Kit (Cat# KK4824Roche). Individual libraries were
724 normalized to 5 nM. NovaSeq 150×150 bp sequencing libraries were chemically denatured and
725 applied to an Illumina NovaSeq flow cell using the XP workflow (20043131). Following transfer to
726 an Illumina NovaSeq 6000 instrument, 150×150 cycle paired-end sequencing was performed
727 using a S4 reagent Kit v1.5 (Cat# 20028312; Illumina). 8-11 million reads were generated per
728 sample and were aligned to the *GRCm38* mouse reference genome. Differential gene expression
729 and pathway analysis were conducted using the DESeq2 and Enrichr R packages.
730
731 **NOD-EAE**
732 15-18 week-old female littermate *Ocab*$^{fl/fl}$ and *Ocab*$^{fl/fl}$;CD4-Cre animals backcrossed to a NOD
733 strain background[30] were used for all experiments. EAE was induced by two 100 μL s.c. injections
734 into both hind flanks of 0.5 μmol/mL MOG_{35-55} peptide emulsified in incomplete Freuds adjuvant
735 (Cat# 77145; ThermoFisher) supplemented with 4 mg/mL heat-killed *M. tuberculosis* (Cat#
736 DF3114338; Fisher Scientific) to form CFA. Animals were given two 400 ng i.p. injections of
737 *Bordetella pertussis* toxin (Cat# 181; List Biological Laboratories) on days 0 and 2. Clinical
738 disease was assessed over 47 days using a 5-point scale described below. Remission timepoints
739 were determined to be between days 22-26 while relapse was determined to be between days
740 26-39.
741
742 **Single-cell RNA-seq**
743 NOD.*Ocab*$^{fl/fl}$ and NOD.*Ocab*$^{fl/fl}$;CD4-Cre animals were induced with EAE and monitored for
744 disease progression. Brains and spinal cords were isolated on day 24 (remission) and day 33
745 (relapse), and processed for FACS sorting. Viable cells were sorted by CD3ε using a FACSAria
746 (BD Bioscience). Cells from each condition were isolated from 3-4 mice and combined. Cells were
747 processed using the 5' 10X Genomics Chromium platform according to the manufacturer's
748 instructions. Paired-end high-throughput sequencing (125 cycles) was performed using a
749 NovaSeq instrument (Illumina). Sequencing reads were processed by using the 10X Genomics

750 CellRanger pipeline and further analyzed using the Seurat R package. Analysis of cells used a
751 standard filtering protocol removing cells with unique feature counts of >5,000 or <100, as well as
752 cells with >10% mitochondrial counts (indicative of dead cells). No more than 10% of total cells
753 were removed by this process. Cells were subjected to unsupervised hierarchical clustering
754 followed by uniform manifold approximation and projection (UMAP) to visualize clusters with
755 similar gene expression and their relative positions. RNA velocity analysis was performed using
756 velocyto.R version 0.6 to model cell state transitions using the guidelines provided in Manno et
757 al.[45] and the associated repository at https://github.com/velocyto-team/velocyto.R. High
758 dimensional velocity vectors were graphed on the predefined Seurat UMAP projection using
759 localized average grid projections. Pseudotime analysis was conducted using Seurat and
760 Monocle3 packages. Integrated data was divided into subset based on genotype and Monocle3
761 was used to calculate trajectory, order cells and plot pseudotime for each condition.
762
763 **Statistics**
764 Multiple two-tailed student's t-tests were used to determine statistical differences in EAE clinical
765 scores and all error bars denote ±SEM unless otherwise noted. Two-way ANOVA was used to
766 determine differences in weight loss throughout disease progression. GraphPad Prism software
767 was used for all statistics and graphing. Two-tailed student's t-tests were used to determine
768 statistical differences in cell populations observed by flow cytometry and all error bars represent
769 ±SD unless otherwise noted. For all figures, ns = $p>0.05$, * = $p\leq0.05$, ** = $p\leq0.01$, *** = $p\leq0.001$,
770 **** = $p\leq0.0001$.

Reporting summary

Information regarding research design is available in the Nature Portfolio Reporting Summary linked to this article.

Data availability

All RNA sequencing, single-cell sequencing, and single-cell T cell V(D)J sequencing data associated with the findings of this study have been deposited to NCBI's GEO database under accession code GSE243727.

Acknowledgements

We thank R.M. O'Connell and M. Bettini for critical reading of the manuscript. We thank J. Marvin and University of Utah Health Sciences Center Flow Cytometry core, and B. Dalley, O. Allen and the High-Throughput Genomics core. Peptides were synthesized by the DNA/Peptide facility. We thank T. Lane for assistance with JHMV constructs, protocols and reagents. This work was supported by grants from the National Institutes of Health/ National Institute of Allergy and Infectious Diseases (R01AI162929 and R01AI100873) and the Praespero Foundation (Canada) to DT, and training grants from the National Institute of Neurological Disorders and Stroke (T32NS115664) to EPH and National Institute of Allergy and Infectious Diseases (T32AI055434) to ARS.

Author contributions

E.P.H. and D.T. conceived the study. E.P.H. and A.S. performed experiments. E.P.H, A.S., E.M.M. and B.T.S. analyzed data. T.E.L., B.T.S. and D.T. provided critical resources and supervision for the study. E.P.H. and D.T. wrote, reviewed and revised the manuscript.

Competing interests

The authors declare that they have no conflicts of interest

798 **References**

799 1. Wallin, M. T. *et al.* The prevalence of MS in the United States. *Neurology* **92**, e1029–
800 e1040 (2019).
801 2. Wtccc, C. C. *et al.* Genetic risk and a primary role for cell-mediated immune mechanisms
802 in multiple sclerosis. *Nature* **476**, 214–219 (2011).
803 3. IMSGC. A high-density screen for linkage in multiple sclerosis. *Am. J. Hum. Genet.* **77**,
804 454–467 (2005).
805 4. Adorini, L., Guery, J.-C. & Trembleau, S. Manipulation of the Th1/Th2 Cell Balance: An
806 Approach to Treat Human Autoimmune Diseases? *Autoimmunity* **23**, 53–68 (1996).
807 5. Langrish, C. L. *et al.* IL-23 drives a pathogenic T cell population that induces autoimmune
808 inflammation. *J. Exp. Med.* **201**, 233–240 (2005).
809 6. Brucklacher-Waldert, V., Stuerner, K., Kolster, M., Wolthausen, J. & Tolosa, E.
810 Phenotypical and functional characterization of T helper 17 cells in multiple sclerosis.
811 *Brain* **132**, 3329–3341 (2009).
812 7. Montes, M. *et al.* Oligoclonal myelin-reactive T-cell infiltrates derived from multiple
813 sclerosis lesions are enriched in Th17 cells. *Clin. Immunol.* **130**, 133–144 (2009).
814 8. Hartmann, F. J. *et al.* Multiple sclerosis-associated IL2RA polymorphism controls GM-
815 CSF production in human TH cells. *Nat. Commun.* **5**, 5056 (2014).
816 9. Scholz, C., Patton, K. T., Anderson, D. E., Freeman, G. J. & Hafler, D. A. Expansion of
817 Autoreactive T Cells in Multiple Sclerosis Is Independent of Exogenous B7 Costimulation.
818 *J. Immunol.* **160**, 1532–1538 (1998).
819 10. Burns, J. B., Bartholomew, B. D. & Lobo, S. T. Isolation of CD45RO+, Memory T Cells
820 Recognizing Proteolipid Protein from Neurologically Normal Subjects. *Cell. Immunol.* **212**,
821 44–50 (2001).
822 11. Pelfrey, C. M. *et al.* Quantification of Self-Recognition in Multiple Sclerosis by Single-Cell
823 Analysis of Cytokine Production. *J. Immunol.* **165**, 1641–1651 (2000).
824 12. Lovett-Racke, A. E. *et al.* Decreased dependence of myelin basic protein-reactive T cells
825 on CD28-mediated costimulation in multiple sclerosis patients. A marker of
826 activated/memory T cells. *J. Clin. Invest.* **101**, 725–730 (1998).
827 13. Lee, H.-G. *et al.* Pathogenic function of bystander-activated memory-like CD4+ T cells in
828 autoimmune encephalomyelitis. *Nat. Commun.* **10**, 709 (2019).
829 14. Williams, J. L. *et al.* Memory cells specific for myelin oligodendrocyte glycoprotein (MOG)
830 govern the transfer of experimental autoimmune encephalomyelitis. *J. Neuroimmunol.*

831 **234**, 84–92 (2011).
832 15. Elyaman, W. *et al.* Distinct Functions of Autoreactive Memory and Effector CD4+ T Cells
833 in Experimental Autoimmune Encephalomyelitis. *Am. J. Pathol.* **173**, 411–422 (2008).
834 16. Maurano, M. T. *et al.* Systematic Localization of Common Disease-Associated Variation
835 in Regulatory DNA. *Science (80-.).* **337**, 1190–1195 (2012).
836 17. Graham, D. S. C., Wong, A. K., McHugh, N. J., Whittaker, J. C. & Vyse, T. J. Evidence for
837 unique association signals in SLE at the CD28–CTLA4–ICOS locus in a family-based
838 study. *Hum. Mol. Genet.* **15**, 3195–3205 (2006).
839 18. van Heel, D. A. Inflammatory bowel disease is associated with a TNF polymorphism that
840 affects an interaction between the OCT1 and NF-kappaB transcription factors. *Hum. Mol.*
841 *Genet.* **11**, 1281–1289 (2002).
842 19. Farh, K. K. *et al.* Genetic and epigenetic fine mapping of causal autoimmune disease
843 variants. *Nature* **518**, 337–343 (2015).
844 20. Shakya, A. *et al.* Oct1 and OCA-B are selectively required for CD4 memory T cell
845 function. *J. Exp. Med.* **212**, 2115–2131 (2015).
846 21. Kim, H. *et al.* T cell-selective deletion of Oct1 protects animals from autoimmune
847 neuroinflammation while maintaining neurotropic pathogen response. *J.*
848 *Neuroinflammation* **16**, 133 (2019).
849 22. Vázquez-Arreguín, K. *et al.* Oct1/Pou2f1 is selectively required for colon regeneration and
850 regulates colon malignancy. *PLOS Genet.* **15**, e1007687 (2019).
851 23. Perovanovic, J. *et al.* Oct1 cooperates with the Smad family of transcription factors to
852 promote mesodermal lineage specification. *Sci. Signal.* **16**, (2023).
853 24. Sebastiano, V. *et al.* Oct1 regulates trophoblast development during early mouse
854 embryogenesis. *Development* **137**, 3551–3560 (2010).
855 25. Hwang, S. S., Kim, L. K., Lee, G. R. & Flavell, R. A. Role of OCT-1 and partner proteins
856 in T cell differentiation. *Biochim. Biophys. Acta - Gene Regul. Mech.* **1859**, 825–831
857 (2016).
858 26. Kim, U. *et al.* The B-cell-specific transcription coactivator OCA-B/OBF-1/Bob-1 is
859 essential for normal production of immunoglobulin isotypes. *Nature* **383**, 542–547 (1996).
860 27. The GAMES Collaborative Group. Linkage disequilibrium screening for multiple sclerosis
861 implicates JAG1 and POU2AF1 as susceptibility genes in Europeans. *J. Neuroimmunol.*
862 **179**, 108–116 (2006).
863 28. Nakamura, M. *et al.* Genome-wide Association Study Identifies TNFSF15 and POU2AF1

864 as Susceptibility Loci for Primary Biliary Cirrhosis in the Japanese Population. *Am. J.*
865 *Hum. Genet.* **91**, 721–728 (2012).
866 29. Sun, W. *et al.* OCA-B/Pou2af1 is sufficient to promote CD4+ T cell memory and
867 prospectively identifies memory precursors. *Proc. Natl. Acad. Sci. U. S. A.* **121**,
868 e2309153121 (2024).
869 30. Kim, H. *et al.* Targeting transcriptional coregulator OCA-B/Pou2af1 blocks activated
870 autoreactive T cells in the pancreas and type 1 diabetes. *J. Exp. Med.* **218**, 133 (2021).
871 31. Tzartos, J. S. *et al.* IL-21 and IL-21 Receptor Expression in Lymphocytes and Neurons in
872 Multiple Sclerosis Brain. *Am. J. Pathol.* **178**, 794–802 (2011).
873 32. Ndhlovu, L. C., Ishii, N., Murata, K., Sato, T. & Sugamura, K. Critical Involvement of
874 OX40 Ligand Signals in the T Cell Priming Events During Experimental Autoimmune
875 Encephalomyelitis. *J. Immunol.* **167**, 2991–2999 (2001).
876 33. Hurwitz, A. A., Sullivan, T. J., Sobel, R. A. & Allison, J. P. Cytotoxic T lymphocyte
877 antigen-4 (CTLA-4) limits the expansion of encephalitogenic T cells in experimental
878 autoimmune encephalomyelitis (EAE)-resistant BALB/c mice. *Proc. Natl. Acad. Sci.* **99**,
879 3013–3017 (2002).
880 34. Arellano, G., Ottum, P. A., Reyes, L. I., Burgos, P. I. & Naves, R. Stage-Specific Role of
881 Interferon-Gamma in Experimental Autoimmune Encephalomyelitis and Multiple
882 Sclerosis. *Front. Immunol.* **6**, (2015).
883 35. Rottman, J. B. *et al.* The costimulatory molecule ICOS plays an important role in the
884 immunopathogenesis of EAE. *Nat. Immunol.* **2**, 605–611 (2001).
885 36. Rouse, M., Nagarkatti, M. & Nagarkatti, P. S. The role of IL-2 in the activation and
886 expansion of regulatory T-cells and the development of experimental autoimmune
887 encephalomyelitis. *Immunobiology* **218**, 674–682 (2013).
888 37. Duncker, P. C., Stoolman, J. S., Huber, A. K. & Segal, B. M. GM-CSF Promotes Chronic
889 Disability in Experimental Autoimmune Encephalomyelitis by Altering the Composition of
890 Central Nervous System–Infiltrating Cells, but Is Dispensable for Disease Induction. *J.*
891 *Immunol.* **200**, 966–973 (2018).
892 38. Yosef, N. *et al.* Dynamic regulatory network controlling TH17 cell differentiation. *Nature*
893 **496**, 461–468 (2013).
894 39. Ikegami, I., Takaki, H., Kamiya, S., Kamekura, R. & Ichimiya, S. Bob1 enhances RORγt-
895 mediated IL-17A expression in Th17 cells through interaction with RORγt. *Biochem.*
896 *Biophys. Res. Commun.* **514**, 1167–1171 (2019).

897 40. Baker, D. *et al.* Autoimmune encephalomyelitis in NOD mice is not initially a progressive
898 multiple sclerosis model. *Ann. Clin. Transl. Neurol.* **6**, acn3.792 (2019).
899 41. Rumble, J. M. *et al.* Neutrophil-related factors as biomarkers in EAE and MS. *J. Exp.*
900 *Med.* **212**, 23–35 (2015).
901 42. Kroenke, M. A., Carlson, T. J., Andjelkovic, A. V. & Segal, B. M. IL-12– and IL-23–
902 modulated T cells induce distinct types of EAE based on histology, CNS chemokine
903 profile, and response to cytokine inhibition. *J. Exp. Med.* **205**, 1535–1541 (2008).
904 43. Grifka-Walk, H. M., Lalor, S. J. & Segal, B. M. Highly polarized Th17 cells induce EAE via
905 a T-bet independent mechanism. *Eur. J. Immunol.* **43**, 2824–2831 (2013).
906 44. Schnell, A. *et al.* Stem-like intestinal Th17 cells give rise to pathogenic effector T cells
907 during autoimmunity. *Cell* **184**, 6281-6298.e23 (2021).
908 45. La Manno, G. *et al.* RNA velocity of single cells. *Nature* **560**, 494–498 (2018).
909 46. Alpsoy, A. *et al.* IκBζ is a dual-use coactivator of NF-κB and POU transcription factors.
910 *Mol. Cell* (2024). doi:10.1016/j.molcel.2024.01.007
911 47. Wu, X. S. *et al.* OCA-T1 and OCA-T2 are coactivators of POU2F3 in the tuft cell lineage.
912 *Nature* **607**, 169–175 (2022).
913 48. Schubart, D. B., Rolink, A., Kosco-Vilbois, M. H., Botteri, F. & Matthias, P. B-cell-specific
914 coactivator OBF-1/OCA-B/Bob1 required for immune response and germinal centre
915 formation. *Nature* **383**, 538–42 (1996).
916 49. Schubart, D. B., Rolink, A., Kosco-Vilbois, M. H., Botteri, F. & Matthias, P. B-cell-specif ic
917 coactivator OBF-1/OCA-B/Bob1 required for immune response and germinal centre
918 formation. *Nature* **383**, 538–542 (1996).
919 50. Qin, X. F., Reichlin, A., Luo, Y., Roeder, R. G. & Nussenzweig, M. C. OCA-B integrates B
920 cell antigen receptor-, CD40L- and IL 4-mediated signals for the germinal center pathway
921 of B cell development. *EMBO J.* **17**, 5066–75 (1998).
922 51. Heng, T. S. P. *et al.* The Immunological Genome Project: networks of gene expression in
923 immune cells. *Nat. Immunol.* **9**, 1091–1094 (2008).
924 52. Zwilling, S., Dieckmann, A., Pfisterer, P., Angel, P. & Wirth, T. Inducible Expression and
925 Phosphorylation of Coactivator BOB.1/OBF.1 in T Cells. *Science (80-.).* **277**, 221–225
926 (1997).
927 53. Gearty, S. V. *et al.* An autoimmune stem-like CD8 T cell population drives type 1
928 diabetes. *Nature* **602**, 156–161 (2022).
929 54. Paroni, M. *et al.* Recognition of viral and self-antigens by T H 1 and T H 1/T H 17 central

930 memory cells in patients with multiple sclerosis reveals distinct roles in immune
931 surveillance and relapses. *J. Allergy Clin. Immunol.* **140**, 797–808 (2017).
932 55. Johns, T. G. *et al.* Myelin oligodendrocyte glycoprotein induces a demyelinating
933 encephalomyelitis resembling multiple sclerosis. *J. Immunol.* **154**, 5536–41 (1995).
934 56. McRae, B. L. *et al.* Induction of active and adoptive relapsing experimental autoimmune
935 encephalomyelitis (EAE) using an encephalitogenic epitope of proteolipid protein. *J.*
936 *Neuroimmunol.* **38**, 229–240 (1992).
937 57. Bernard, C. C. A. *et al.* Myelin oligodendrocyte glycoprotein: a novel candidate
938 autoantigen in multiple sclerosis. *J. Mol. Med.* **75**, 77–88 (1997).
939 58. Anderson, A. C. *et al.* A Transgenic Model of Central Nervous System Autoimmunity
940 Mediated by CD4+ and CD8+ T and B Cells. *J. Immunol.* **188**, 2084–2092 (2012).
941 59. Nish, S. A. *et al.* CD4+ T cell effector commitment coupled to self-renewal by asymmetric
942 cell divisions. *J. Exp. Med.* **214**, 39–47 (2017).
943 60. Mammadli, M., Suo, L., Sen, J. M. & Karimi, M. TCF-1 Is Required for CD4 T Cell
944 Persistence Functions during AlloImmunity. *Int. J. Mol. Sci.* **24**, 4326 (2023).
945 61. Kadowaki, A., Saga, R., Lin, Y., Sato, W. & Yamamura, T. Gut microbiota-dependent
946 CCR9+CD4+ T cells are altered in secondary progressive multiple sclerosis. *Brain* **142**,
947 916–931 (2019).
948 62. Thakore, P. I. *et al.* The chromatin landscape of Th17 cells reveals mechanisms of
949 diversification of regulatory and pro-inflammatory states. *BioRxiv* (2022).
950 63. Song, S. *et al.* OBF1 and Oct factors control the germinal center transcriptional program.
951 *Blood* **137**, 2920–2934 (2021).
952 64. Sha, Y. & Markovic-Plese, S. Activated IL-1RI Signaling Pathway Induces Th17 Cell
953 Differentiation via Interferon Regulatory Factor 4 Signaling in Patients with Relapsing-
954 Remitting Multiple Sclerosis. *Front. Immunol.* **7**, (2016).
955 65. Lane, T. E. *et al.* A Central Role for CD4 + T Cells and RANTES in Virus-Induced Central
956 Nervous System Inflammation and Demyelination. *J. Virol.* **74**, 1415–1424 (2000).
957 66. Blanc, C. A. *et al.* Sphingosine-1-Phosphate Receptor Antagonism Enhances
958 Proliferation and Migration of Engrafted Neural Progenitor Cells in a Model of Viral-
959 Induced Demyelination. *Am. J. Pathol.* **185**, 2819–2832 (2015).
960 67. Plaisted, W. C. *et al.* Remyelination Is Correlated with Regulatory T Cell Induction
961 Following Human Embryoid Body-Derived Neural Precursor Cell Transplantation in a
962 Viral Model of Multiple Sclerosis. *PLoS One* **11**, e0157620 (2016).

963 68. Ray, A. & Dittel, B. N. Isolation of mouse peritoneal cavity cells. *J. Vis. Exp.* (2010).
964 doi:10.3791/1488
965 69. Lane, T. E. *et al.* A central role for CD4(+) T cells and RANTES in virus-induced central
966 nervous system inflammation and demyelination. *J. Virol.* **74**, 1415–24 (2000).
967 70. Dickey, L. L., Worne, C. L., Glover, J. L., Lane, T. E. & O'Connell, R. M. MicroRNA-155
968 enhances T cell trafficking and antiviral effector function in a model of coronavirus-
969 induced neurologic disease. *J. Neuroinflammation* **13**, 240 (2016).
970

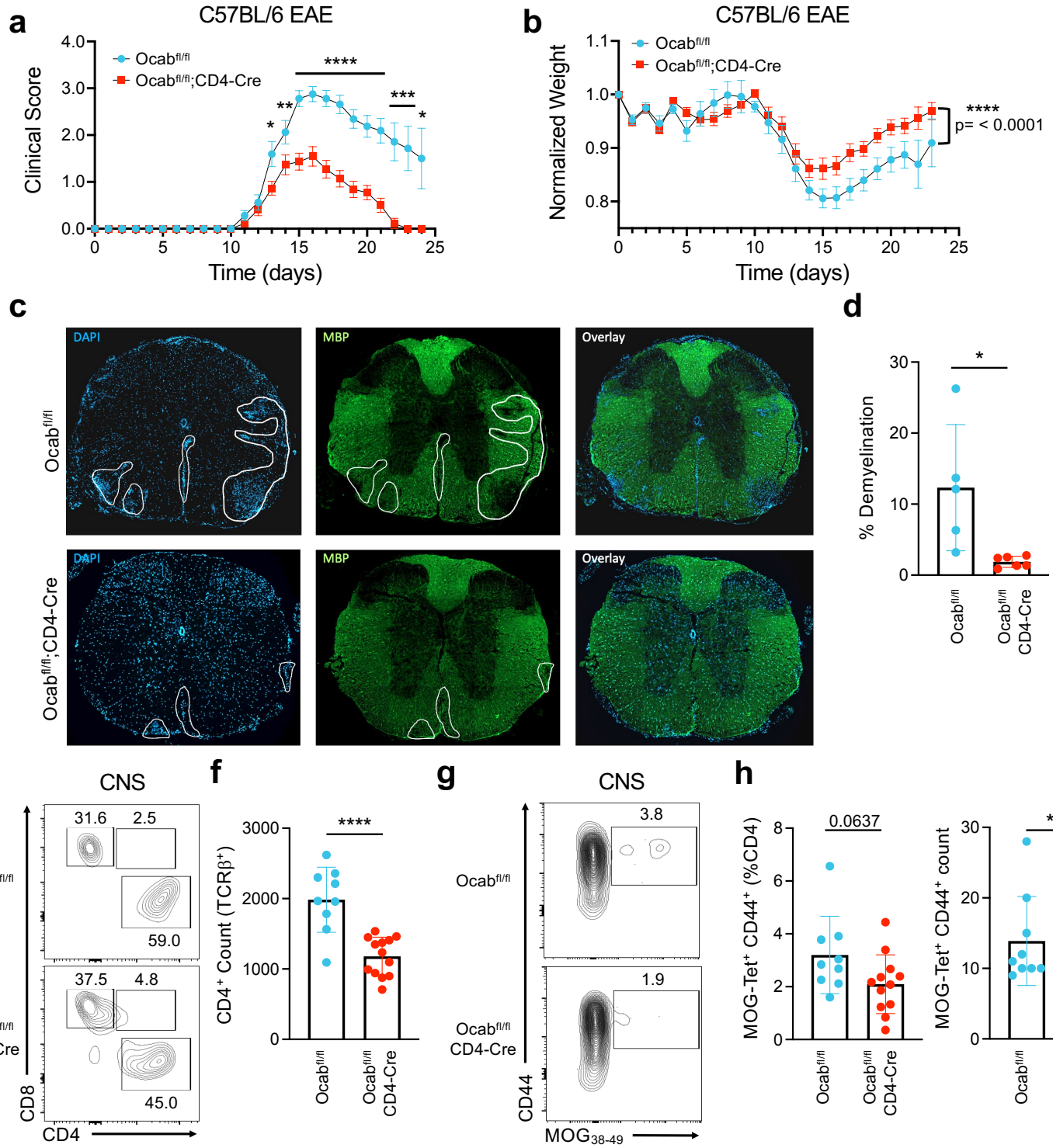
a
C57BL/6 EAE
Clinical Score
Time (days)
Ocab fl/fl
Ocab fl/fl;CD4-Cre
****
***
**
*
b
C57BL/6 EAE
Normalized Weight
Time (days)
Ocab fl/fl
Ocab fl/fl;CD4-Cre
****
p= < 0.0001
c
DAPI
MBP
Overlay
Ocab fl/fl
Ocab fl/fl;CD4-Cre
d
% Demyelination
*
Ocab fl/fl
Ocab fl/fl CD4-Cre
e
CNS
31.6
2.5
59.0
37.5
4.8
45.0
Ocab fl/fl
Ocab fl/fl CD4-Cre
CD8
CD4
f
CD4+ Count (TCRβ+)
****
Ocab fl/fl
Ocab fl/fl CD4-Cre
g
CNS
3.8
1.9
Ocab fl/fl
Ocab fl/fl CD4-Cre
CD44
MOG38-49
h
MOG-Tet+ CD44+ (%CD4)
0.0637
MOG-Tet+ CD44+ count
**
Ocab fl/fl
Ocab fl/fl CD4-Cre

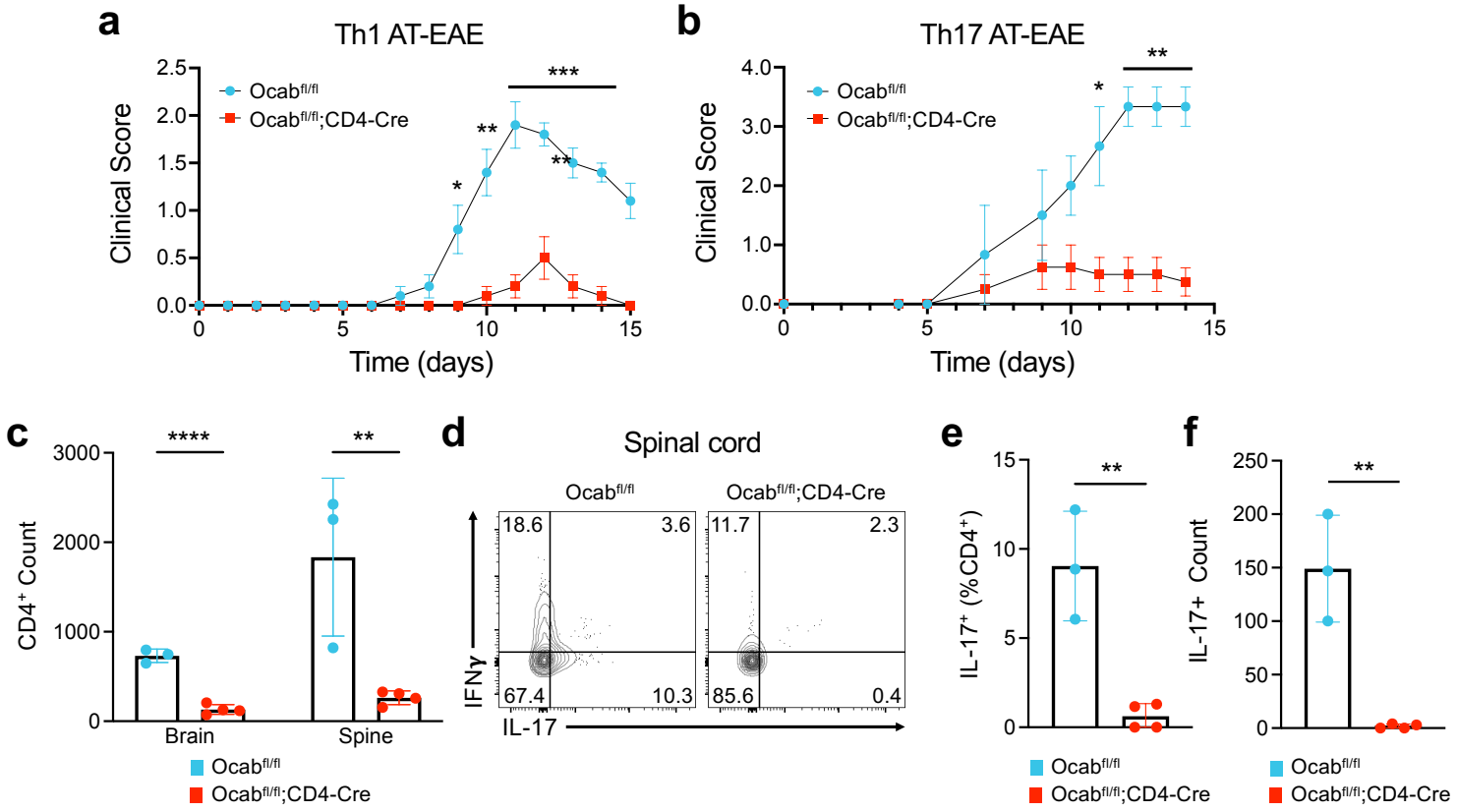
a
Th1 AT-EAE
Clinical Score
Time (days)
Ocab$^{fl/fl}$
Ocab$^{fl/fl}$;CD4-Cre
b
Th17 AT-EAE
Clinical Score
Time (days)
Ocab$^{fl/fl}$
Ocab$^{fl/fl}$;CD4-Cre
c
CD4$^+$ Count
Brain
Spine
Ocab$^{fl/fl}$
Ocab$^{fl/fl}$;CD4-Cre
d
Spinal cord
Ocab$^{fl/fl}$
Ocab$^{fl/fl}$;CD4-Cre
IFNγ
IL-17
18.6
3.6
67.4
10.3
11.7
2.3
85.6
0.4
e
IL-17$^+$ (%CD4$^+$)
Ocab$^{fl/fl}$
Ocab$^{fl/fl}$;CD4-Cre
f
IL-17+ Count
Ocab$^{fl/fl}$
Ocab$^{fl/fl}$;CD4-Cre

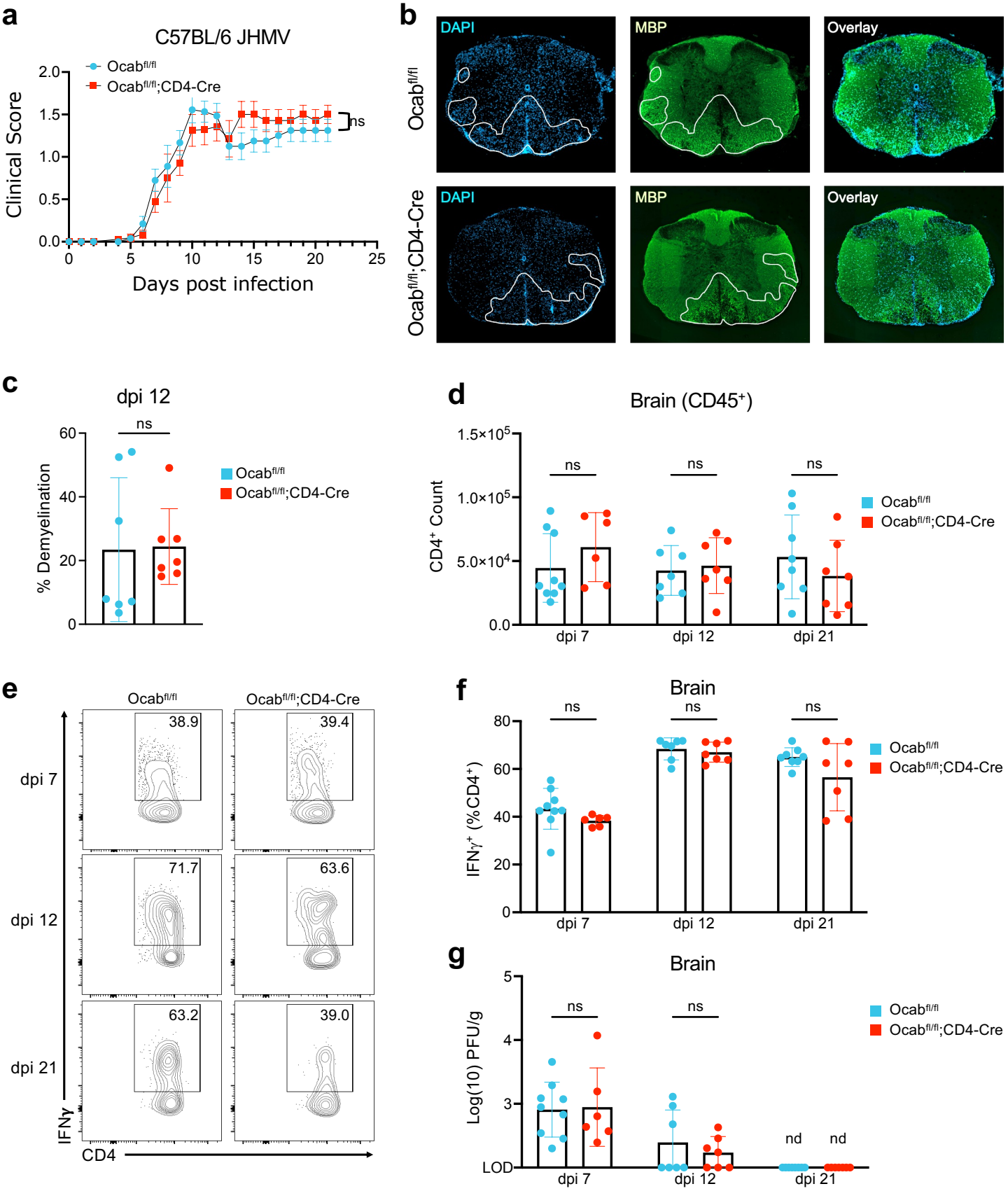
a
C57BL/6 JHMV
Ocab$^{fl/fl}$
Ocab$^{fl/fl}$;CD4-Cre
Clinical Score
Days post infection
ns
b
DAPI
MBP
Overlay
Ocab$^{fl/fl}$
Ocab$^{fl/fl}$;CD4-Cre
c
dpi 12
% Demyelination
ns
d
Brain (CD45$^+$)
CD4$^+$ Count
dpi 7
dpi 12
dpi 21
e
Ocab$^{fl/fl}$
Ocab$^{fl/fl}$;CD4-Cre
38.9
39.4
71.7
63.6
63.2
39.0
IFNγ
CD4
f
Brain
IFNγ$^+$ (%CD4$^+$)
g
Brain
Log(10) PFU/g
LOD
nd

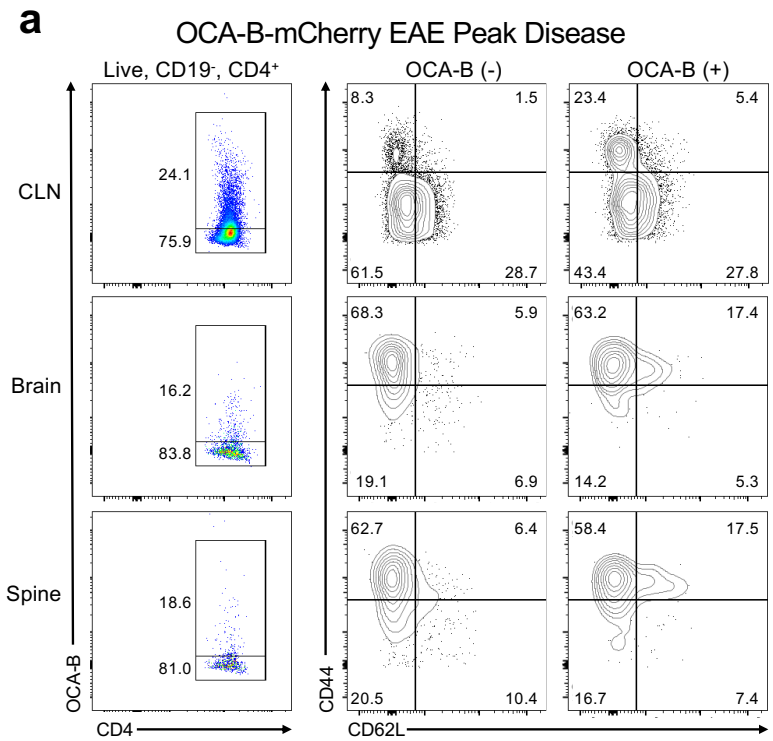

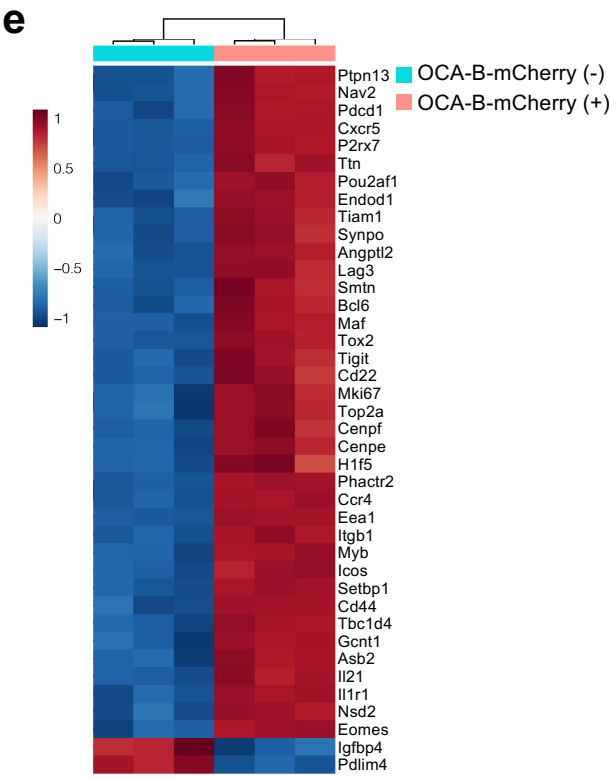

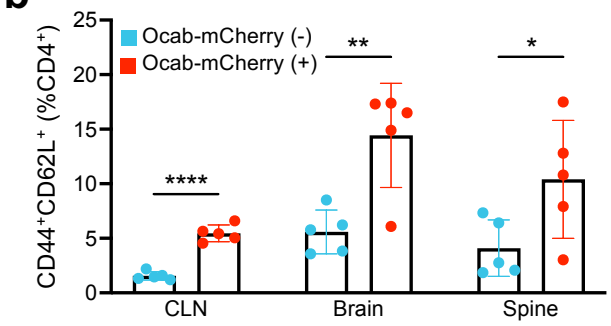

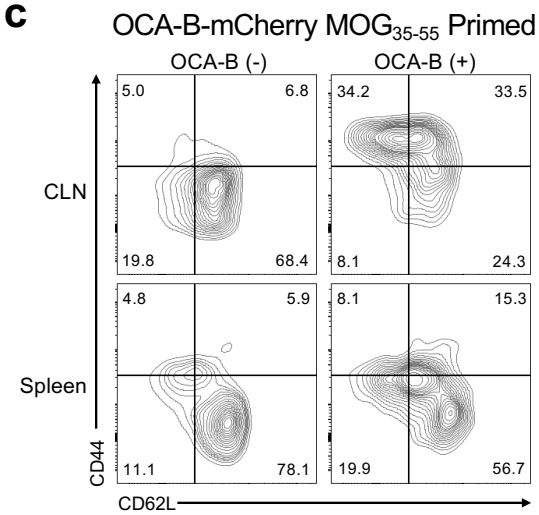

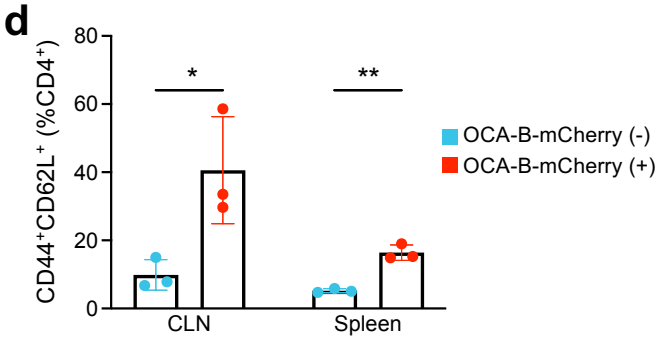

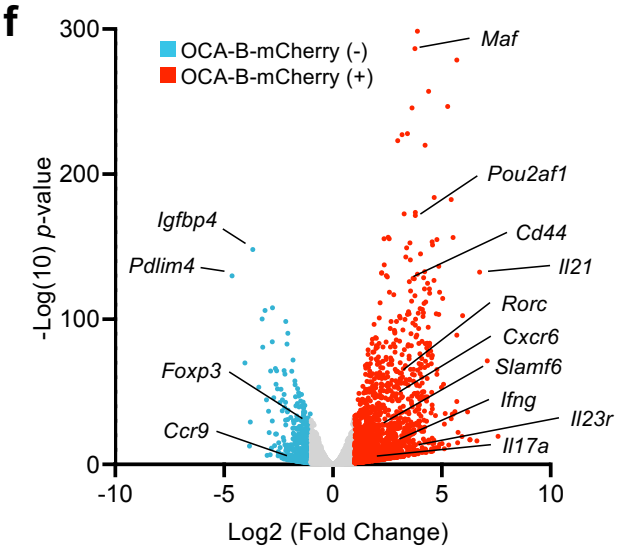

g

OCA-B+ Enriched Pathways

KEGG Pathway	*p*-value
Systemic Lupus Erythematosus	1.02E-04
Cytokine Cytokine Receptor Interaction	5.04E-04
Autoimmune Thyroid Disease	1.16E-03
Type I Diabetes Mellitus	2.06E-03

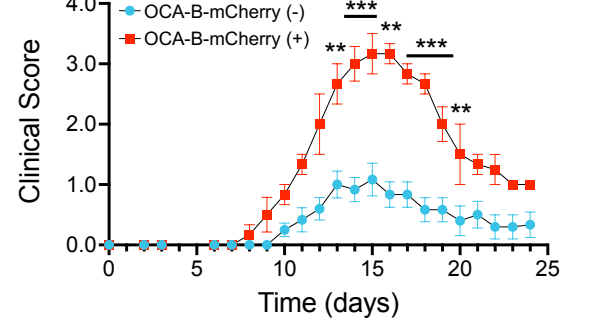

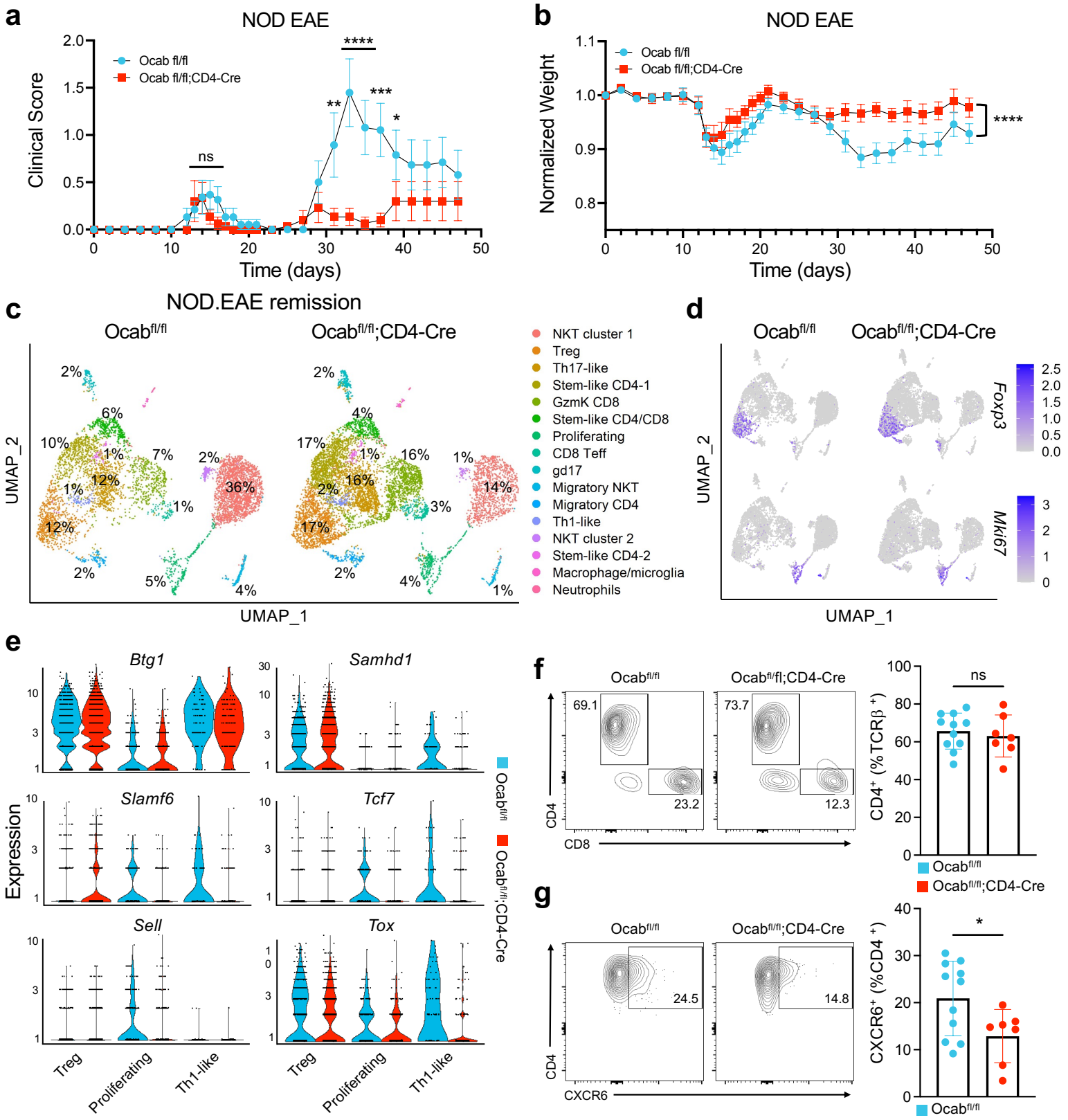
a
NOD EAE
Clinical Score
Time (days)
Ocab fl/fl
Ocab fl/fl;CD4-Cre
ns
**
***
****
*
b
NOD EAE
Normalized Weight
Time (days)
Ocab fl/fl
Ocab fl/fl;CD4-Cre
****
c
NOD.EAE remission
Ocabfl/fl
Ocabfl/fl;CD4-Cre
UMAP_2
UMAP_1
NKT cluster 1
Treg
Th17-like
Stem-like CD4-1
GzmK CD8
Stem-like CD4/CD8
Proliferating
CD8 Teff
gd17
Migratory NKT
Migratory CD4
Th1-like
NKT cluster 2
Stem-like CD4-2
Macrophage/microglia
Neutrophils
d
Ocabfl/fl
Ocabfl/fl;CD4-Cre
Foxp3
Mki67
UMAP_2
UMAP_1
e
Btg1
Samhd1
Slamf6
Tcf7
Sell
Tox
Expression
Treg
Proliferating
Th1-like
Ocabfl/fl
Ocabfl/fl;CD4-Cre
f
Ocabfl/fl
Ocabfl/fl;CD4-Cre
69.1
23.2
73.7
12.3
CD4
CD8
ns
CD4+ (%TCRβ+)
Ocabfl/fl
Ocabfl/fl;CD4-Cre
g
Ocabfl/fl
Ocabfl/fl;CD4-Cre
24.5
14.8
CD4
CXCR6
*
CXCR6+ (%CD4+)
Ocabfl/fl
Ocabfl/fl;CD4-Cre
h
Ocabfl/fl
Ocabfl/fl;CD4-Cre
77.4
6.9
55.8
3.6
IFNγ
GM-CSF
i
ns
IFNγ+GM-CSF- (%CD4+)
*
IFNγ+GM-CSF+ (%CD4+)
Ocabfl/fl
Ocabfl/fl;CD4-Cre

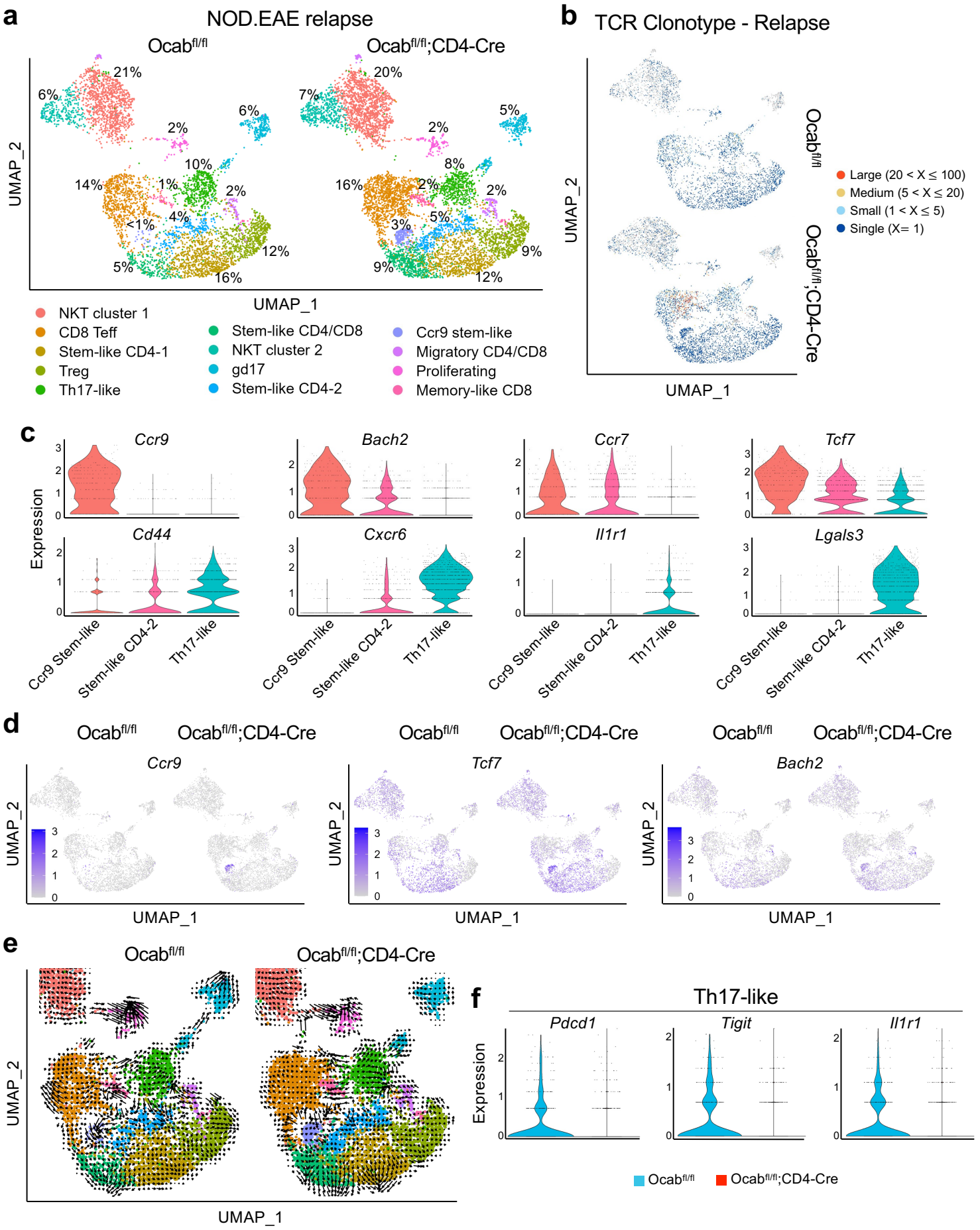
a
NOD.EAE relapse
Ocab fl/fl
Ocab fl/fl;CD4-Cre
UMAP_2
UMAP_1
21%
6%
2%
6%
10%
14%
1%
2%
<1%
4%
12%
5%
16%
20%
7%
2%
5%
8%
16%
2%
2%
3%
5%
9%
9%
12%
NKT cluster 1
CD8 Teff
Stem-like CD4-1
Treg
Th17-like
Stem-like CD4/CD8
NKT cluster 2
gd17
Stem-like CD4-2
Ccr9 stem-like
Migratory CD4/CD8
Proliferating
Memory-like CD8
b
TCR Clonotype - Relapse
Ocab fl/fl
Ocab fl/fl;CD4-Cre
Large (20 < X ≤ 100)
Medium (5 < X ≤ 20)
Small (1 < X ≤ 5)
Single (X= 1)
c
Ccr9
Bach2
Ccr7
Tcf7
Cd44
Cxcr6
Il1r1
Lgals3
Expression
Ccr9 Stem-like
Stem-like CD4-2
Th17-like
d
Ccr9
Tcf7
Bach2
e
f
Th17-like
Pdcd1
Tigit
Il1r1
Ocab fl/fl
Ocab fl/fl;CD4-Cre